

## Exploring hurricane wind speed along US Atlantic coast in warming climate and effects on predictions of structural damage and intervention costs

Wei Cui, Luca Caracoglia \*

*Department of Civil and Environmental Engineering, Northeastern University, Boston, MA 02115, USA*



### ARTICLE INFO

**Article history:**

Received 23 July 2015

Revised 29 December 2015

Accepted 2 May 2016

Available online 26 May 2016

**Keywords:**

Hurricane hazard

Climate change

Sea surface temperature

Hurricane track

Hurricane frequency

Wind speed

Performance-based wind engineering

Intervention costs

Tall buildings

### ABSTRACT

This paper proposes a methodology for the rational assessment of lifetime costs on tall buildings due to hurricane-induced damage along the US Atlantic coastline accounting for plausible future warming climate scenarios. The hurricane simulation is based on Vickery's empirical model. Initially, regression errors in Vickery's model are discussed; some adjustments are proposed to enable hurricane simulation in future climates. After verification of the hurricane model's ability to simulate the results of the United States historical hurricane database, simulation of hurricane activity in future climates is examined. The warming climate scenarios are reproduced from the results of the community earth system model, maintained by the National Center for Atmospheric Research (NCAR). Three different future climate scenarios, RCP2.6, RCP4.5 and RCP8.5, are considered. The influence of warming climate on two quantities, relevant to wind engineering, is examined: hurricane frequency and hurricane intensity. It is found that, in a warming climate environment, the hurricane frequency and hurricane intensity may vary depending on the RCP scenario. Therefore, the probability distribution of the wind speed in hurricane-prone areas of the United States, both coastal and interior areas, will also be influenced by the RCPs.

The numerical methodology for computing wind speed probability distribution in a future warming climate, influenced by the various RCP scenarios, is subsequently coupled with an existing approach for structural performance analysis against wind hazards to predict the indirect effect of future warming climate on the structural intervention costs (i.e. repair costs), induced by the damaging winds. A 180-m tall benchmark building, located in Miami (Florida, USA), is used as one example of application in conjunction with a series of structural fragility curves, derived from a recent study for the same structure. The evaluation of lifetime intervention costs is later expanded to demonstrate the ability of the proposed methodology to predict hurricane wind damage, if the location of the structure is moved to several other cities along the Atlantic coast of the United States.

© 2016 Elsevier Ltd. All rights reserved.

### 1. Introduction

Hurricanes are among the most destructive weather phenomena, which can cause severe damage to structures and loss of human lives due to strong winds and surge effects. In 2005, Hurricane Katrina caused 1833 fatalities and \$108 billion property damage in several coastal regions along the Gulf of Mexico. In 2012, Hurricane Sandy led to about \$65 billion damage in the northeastern coastal region of the USA and in the Ontario Province of Canada. The severity of the consequences, associates with

hurricane activity, has motivated several investigations, attempting to forecast hurricane activity in both near and distant future. A short review of the most important models, currently employed for hurricane simulation in wind engineering, is provided in the following section. For example, Georgiou derived a pioneering method to numerically model the hurricane wind field and to predict wind speed in a hurricane along the US Atlantic coast [1]. Simiu proposed a "single-site" probabilistic model, which employs Monte Carlo simulation to compute hurricane reference wind speeds as a function of five random quantities or parameters [2]. Subsequently, Vickery proposed an empirical track model [3,4], derived from statistical linear regression of a large hurricane database. This model has been comprehensively validated and widely used for long-term hurricane wind field predictions. The initial model by Vickery has been upgraded a number of times to advance the prediction of

\* Corresponding author at: Department of Civil and Environmental Engineering, Northeastern University, 400 Snell Engineering Center, 360 Huntington Avenue, Boston, MA 02115, USA. Tel.: +1 617 (373) 5186; fax: +1 617 (373) 4419.

E-mail address: [lucac@coe.neu.edu](mailto:lucac@coe.neu.edu) (L. Caracoglia).

hurricane wind speeds [5–8] and it is currently employed in its latest form to generate the wind speed maps in the ASCE-7 civil engineering design standard [9].

In recent years various physical observations have been attributed to the effect of “climate change” by the research community, governments and society. These include, for example, melting of glaciers, an increasing hurricane activity and longer periods of drought. Since the publication of the First Assessment Report by the Intergovernmental Panel on Climate Change (IPCC) in 1990 [10], scientists indicate that it is extremely likely (at least 95% probability) that humans are contributing to these effects because of a larger concentration of greenhouse gases in the atmosphere [11]. The current theories [11] tend to suggest that the surface temperature may continue to increase in the 21st century and other climate indicators may also progressively change.

One of the consequences, attributed to climate change by researchers [12,13], is the potential change in hurricane number, duration and intensity. Analysis of the hurricane history in the North Atlantic Ocean indicates that the annual number of hurricanes, especially intense hurricanes, has been increasing in the last century [13]. The relationship between sea temperature and hurricane frequency may lead to the following conclusion: the sea surface temperature (SST), i.e. the power source of hurricanes, may influence hurricane genesis frequency, hurricane genesis spatial location, intensity and trajectory path. Thus, it has been suggested that the increasing SST may likely be correlated with the recent unusual hurricane activity in the North Atlantic Ocean [12].

Consequently, it is relevant for the structural engineer to examine the influence of climate change on structural integrity and to possibly consider the concept of “adaption” in the design process. The significance of climate change and adaptation in structural engineering is for example demonstrated by several recent studies on the deterioration of civil structures [14–16]. In the field of wind engineering attention has been paid to the advancement of structural design standards for wind loads, predominantly considering a traditional prescriptive approach [17]. The concept of performance-based approach for structural design has been investigated in wind engineering both for low-rise buildings (e.g., [18–20]), tall buildings (e.g., [21–26]) and long-span bridges (e.g., [27,28]). In recent years several studies have analyzed the effects generated by SST variations, for example promoted by climate change, on the extreme value distribution of the hurricane wind speed [17,29–31]. Research activities have considered the fundamental research question about the correlation between plausible climate change scenarios, SST variations and hurricane extreme wind speed distributions [17,29,30,32,31]. Nevertheless, very few results are available on the indirect effects of such climatic variations on the built environment (e.g., [30,32]).

This research is a continuation of a research activity on the evaluation of lifetime monetary losses due to hurricane-induced damage on tall buildings [24]. This study proposes, for the first time, a numerical methodology for assessing monetary losses, incurred by the owner of a tall building, due to the rising hurricane threat accounting for a progressively warming climate. The aim of this research is not the examination of the connection between the current IPCC model predictions and the role of SST variations on the increased hurricane intensity. On the contrary, this study proposes to “bridge the gap” between the current research activities in climatology, weather extremes and climate change in wind engineering [17,29,30,32] and the crucial issue of the potential indirect consequences on the built environment and, in particular, the damage on the facade of a tall building in structural engineering. This research attempts to evaluate the relative variation of intervention costs due to hurricane-induced damage on a benchmark structure with and without the indirect effect of a future warming climate, given the “best estimate” of

the SST variations indicated by current theories and models on climate change [11].

## 2. Background

### 2.1. Review of IPCC's forecast of increasing SST in the 21st century

In the fifth assessment report by IPCC, the global mean surface temperature has progressively increased since the late 19th century [11], according to recent climate observations. In the future, warmer temperature extremes will likely be present in many areas of the Earth as global mean temperature tends to increase.

In order to establish a common baseline measure for the comparison among various climate model results, Representative Concentration Pathways (RCPs) have been used by IPCC to provide a more quantitative information on the possible “trajectories” of the main forcing agents responsible for climate change [33]. Currently, four RCP values are used by the climate models: RCP8.5, RCP6, RCP4.5 and RCP2.6. Generally, the four RCP values represent four plausible future climate scenarios, which are illustrated in Fig. 1. The scenarios are defined in accordance with a possible range of radiative forcing values in the year 2100 relative to pre-industrial values: +2.6, +4.5, +6.0 and +8.5 W/m<sup>2</sup> [33].

From around the mid-21st century, the rate of global warming appears to be more strongly dependent on the RCP scenarios. The projections of global mean temperature are illustrated in Fig. 1. Solid lines indicate the mean temperatures predicted by various models and the colored areas are the 90% confidence intervals. Since the number of models used in the various reference time

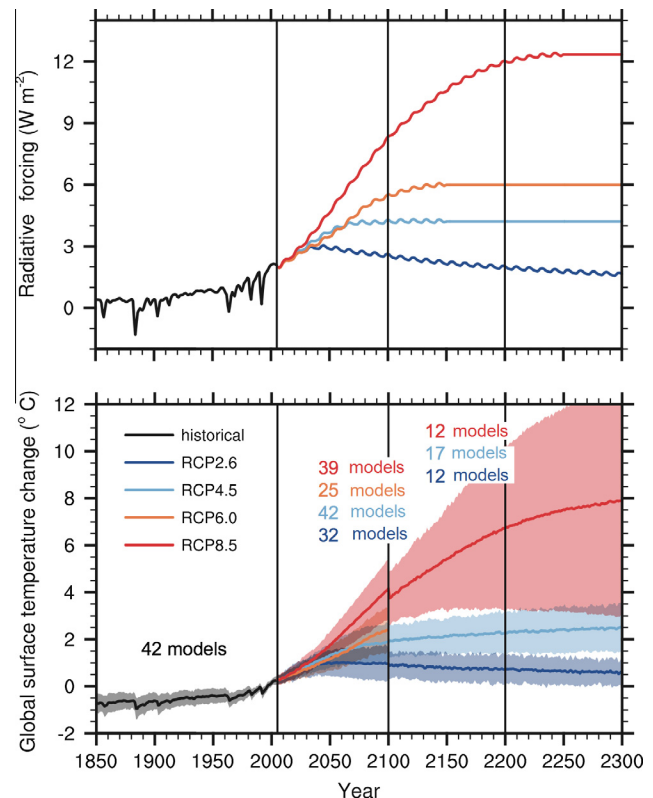


**Fig. 1.** Projections of total global mean radiative forcing (top) and global annual mean surface air temperature anomalies (bottom) in the 21st century and later, with reference to the average temperature in the period 1986–2005. Curves are reproduced from IPCC report [11]. (The integer numbers on the figure panel indicate the number of models used to generate the results for each RCP scenario in various time periods.)

periods (e.g., 1820–2000, 2000–2100, 2100+) are different, some discontinuities are visible along the mean temperature lines at the beginning of a new period in Fig. 1. Because the RCP6.0 scenario has been recently added by IPCC [11], much fewer models are used to generate the results, compared with other scenarios, and no prediction is available after 2100. Therefore, RCP2.6, 4.5 and 8.5 are exclusively considered in this paper.

## 2.2. Potential influence of increasing SST on hurricane activity

The SST plays a key role in the life cycle of hurricanes, from their formation to their evolution and then death. It has been demonstrated that hurricane frequency and intensity may vary as a result of fluctuating SST values [34].

Hurricanes form over tropical sea waters in areas of high humidity, light winds and warm surface temperature (typically, 26.5 °C or greater). As a result, most hurricanes are usually generated in the region of latitude between 8°N and 20°N. Warm temperature conditions usually prevail in the summer and early fall months in the tropical North Atlantic Ocean. For this reason, the hurricane season in the northern hemisphere runs from June until November. If a progressive SST increment in the near future is postulated, the Main Development Region (MDR) of hurricanes [35], where hurricanes originate, may expand to the north and the duration of the hurricane “season” may be prolonged. As a consequence, the hurricane frequency in future years may increase [12]. Recently, researchers have assumed that the mean annual frequency of hurricanes in the North Atlantic Ocean will increase in the 21st century from the examination of the historical hurricane database (HurDat) [17,27,30]. Nevertheless, it must be noted that the HurDat record is partially incomplete due to technical challenges, especially in the early years of hurricane recognition. In addition, Ref. [29] explicitly discusses these issues, and advises to use only land-falling hurricane records instead of the complete HurDat database. Further discussion on the future projection of the hurricane frequency, based on the records of the HurDat database, is presented later in Section 6.1.

Besides the increasing hurricane frequency, the hurricane intensity is correlated with SST. Therefore, it is believed that there will be more intense hurricanes in a future warming climate, as concluded by several studies [17,29]. On the other hand, the study [36] examined the relationship between SST and the rates of intense hurricane land-falling; a small influence of SST on hurricane intensity was observed and very limited correlation between the landfall rate and SST was only noted. Nevertheless, it is still plausible that, if the global temperature increases as predicted by the current trends, there will be more intense hurricanes with stronger winds in the North Atlantic Ocean, affecting the eastern coastline of the United States.

## 2.3. Long-term hurricane wind speed prediction over the US coastline

The synthetic simulation of hurricanes is a widely employed approach for constructing wind speed hazard maps and assessing hurricane risk in structural engineering. This approach has been adopted by design standards in several countries and by the insurance industry [37].

Basically, there are two methods for the numerical simulation of hurricane landfall frequency and minimum pressure: single-site probabilistic model and hurricane track model [2]. The former method is based on five random parameters, the probabilistic properties of which are specified for each single individual location; these are central pressure deficit, radius to maximum winds (RMW), heading of the hurricane, translation speed and the coast crossing position. Given the probability distributions of these parameters, which are derived from hurricane landfall history

and statistics in the vicinity of the selected location, the Monte Carlo method is employed to sample each parameter and to simulate the maximum wind speed from a plausible population of land-falling hurricanes. After landing, hurricanes will move inland along a straight line by progressively decaying their intensity (wind speed), according to a filling rate model [38].

The latter method, first published in [3], combines an empirical data-driven statistical approach with physical evidence. The method uses linear statistical regression to model the hurricane trajectories and intensities. Subsequently, the hurricane wind field model and wind speed are derived from physical theory [4]. The original model has been subsequently refined and upgraded in a series of additional studies [5,6,7,39,37]. Since the hurricane track model has usually been preferred for hurricane risk assessment, it has been selected in this paper as the reference model for the simulation of hurricane activity in a future warming climate.

## 2.4. Application of uncertainty analysis to examine hurricane wind damage to tall buildings and structural lifetime intervention cost

Over the past years, more rational approaches for performance-based design in wind engineering have been examined by several researchers [23,24,28]. The fundamental idea of performance-based design is to increase the flexibility in the design process [40]. These approaches ensure that a building, for example subjected to different wind hazard levels (as opposed to the largest event), can achieve a selected performance objective level [41] by taking into account various sources of uncertainty, either in the load or the structure. Recent studies at Northeastern University [24,42,43] have suggested, as an important source of uncertainty, the variability in the measurements of aerodynamic parameters related to wind loads. Consequently, a number of methodologies have been proposed to evaluate structural fragility curves, which are employed to characterize the vulnerability of tall buildings (and long-span bridges) to extreme wind loads. A typical example of structural fragility curve is illustrated in Fig. 2, reproduced from [24]. A brief summary of the method for uncertainty and structural fragility analysis is provided in this section; more details may be found in [24].

Several limit states have been examined for serviceability type analysis, which has been shown to be important for tall buildings during high winds (for example, wind damage to nonstructural components on the facade [42,24]). The fragility curve in Fig. 2 analyzes the limit states of the root mean square (RMS) acceleration and peak drift/displacement at the rooftop of a benchmark tall building as a function of the reference mean wind speed  $\bar{U}(h)$ . The graph is divided into three regions. In Region I the vulnerability is approximately zero for both limit states. In Region III the

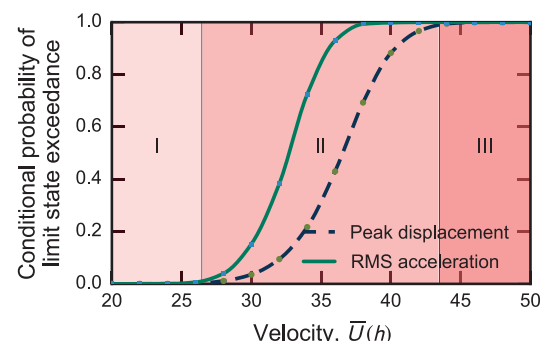


**Fig. 2.** Example of fragility curve (probability of “failure”) as a function of reference mean wind speed  $\bar{U}(h)$ , employed for tall building serviceability analysis during high winds (RMS acceleration and peak drift/displacement at the rooftop).

vulnerability is nearly 1 for both limit states. In Region II the vulnerability varies from 0 to 1, which means that in this range of  $\bar{U}(h)$  the wind-induced structural damage is probabilistic rather than deterministic.

The fragility curves are later combined to predict damage-induced monetary losses over the structural lifetime, either the design life of a new structure or the remaining life of an existing structure. The expected total intervention cost  $C(t)$ , excluding regular periodic maintenance, can be expressed as a function of time  $t$  (years) as follows [44]:

$$E[C(t)] = C_0 + E \left[ \sum_{i=1}^{N(t)} \sum_{j=1}^k C_j e^{-\xi t_i} P_j \right] \quad (1)$$

In the previous equation,  $E[\cdot]$  denotes expected value;  $C_0$  is the initial construction cost;  $i$  is an integer index designating the occurrence of the hazards over time;  $t_i$  is the time at which the  $i$ -th hazard occurs, which is a random variable;  $N(t)$  is the total number of hazard occurrences at time  $t$ ;  $j$  is the index used to designate the various limit states;  $k$  is the total number of design limit states;  $C_j$  are the intervention costs in present dollar value of the  $j$ -th limit state being reached or exceeded at time  $t_i$ ;  $\xi$  is a constant discount rate per year;  $P_j$  is the exceedance probability of the  $j$ -th limit state.

The previous Eq. (1) was first employed to examine structural damage induced by large earthquakes [44] and the variable  $N(t)$  was modeled as a Poisson process for rare events with prescribed arrival rate, which is usually much smaller than one. More discussion on the variable  $N(t)$  is presented in Section 3.4.

If the evaluation of lifetime intervention costs against hurricane damage is needed for a tall building, Eq. (1) must be adapted to comply with the features of hurricanes, since in the hurricane-prone regions of the United States (such as Florida or the coastal areas in the Gulf of Mexico) hurricane hazard occurs almost every year. Therefore, in this study, the counting variable  $N(t)$  may be approximated as increasing numbers from 1 to  $t$ . Consequently,  $P_j$  becomes the annual exceedance probability of the  $j$ -th limit state.

It is also convenient to rewrite Eq. (1) and to obtain the relative average intervention cost  $C_{M,E}$ , which is the expected cost value normalized to the initial construction cost  $C_0$  [28]:

$$C_{M,E} = E \left[ \frac{C(t) - C_0}{C_0} \right] = E \left[ \sum_{i=1}^{N(t)} \sum_{j=1}^k \epsilon_{C,j} e^{-\xi t_i} P_j \right] \quad (2)$$

where  $\epsilon_{C,j} = C_j/C_0$  is the ratio between the intervention cost consequent to “failure” in the  $j$ -th limit state and the initial construction cost  $C_0$ . The estimation of the cost variables  $C_j$  in Eq. (1) and  $\epsilon_{C,j}$  in Eq. (2) is discussed in a previous study [44].

As described above, in Fig. 2 two limit states are employed to examine the performance of a benchmark tall building against high winds: lateral deformation (drift) and acceleration at the rooftop of the building [24]. Therefore, in Eq. (2) and in the remainder of this study  $k = 2$  is used, with  $j = 1$  designating the peak deformation limit state and  $j = 2$  denoting the RMS acceleration limit state.

### 3. Vickery's empirical storm track model

#### 3.1. Track-model equations

The track model by Vickery et al. [3] simulates the storm translation velocity, heading, and hurricane relative intensity. These quantities are expressed in Eqs. (3)–(5):

$$\Delta \ln c = a_1 + a_2 \psi + a_3 \lambda + a_4 \ln c_i + a_5 \theta_i + \epsilon_c \quad (3)$$

$$\Delta \theta = b_1 + b_2 \psi + b_3 \lambda + b_4 c_i + b_5 \theta_i + b_6 \theta_{i-1} + \epsilon_\theta \quad (4)$$

$$\ln(I_{i+1}) = c_0 + c_1 \ln(I_i) + c_2 \ln(I_{i-1}) + c_3 \ln(I_{i-2}) + c_4 T_s + c_5 (\Delta T_s) + \epsilon_I \quad (5)$$

In Eq. (3)  $a_j (j = 1, 2, \dots, 5)$  are coefficients that can be found by linear regression; the  $b_j (j = 1, 2, \dots, 6)$  terms in Eq. (4) are also found by linear regression. The quantities  $\psi$  and  $\lambda$  are latitude and longitude of the hurricane center,  $c_i$  is the hurricane translation speed at time step  $i$ ;  $\theta_i$  is the hurricane heading (direction) at time step  $i$  and  $\theta_{i-1}$  is the hurricane heading at time step  $i - 1$ . The limits of  $\theta$  are  $-180 < \theta \leq 180$ ; when a hurricane heads north,  $\theta = 0$  ( $\theta$  increases counter-clockwise).

In Eq. (5), the relative intensity  $I$  [45], defined at various time steps  $i, i - 1$ , etc., is used as a dimensionless term that relates the actual hurricane pressure deficit  $\Delta p$  to the greatest possible central pressure deficit allowed by the average climatology of the hurricane season [3]. The benefits of introducing SST into the modeling process reduce some of the unexplained variability in the central pressure modeling [3]. The quantity  $T_s$  is the SST at time step  $i + 1$ ;  $\Delta T_s$  is the SST difference between time step  $i$  and time step  $i + 1$ , which is calculated as  $\Delta T_s = T_{s_{i+1}} - T_{s_i}$ . The increments of heading and translation velocity between time step  $i$  and time step  $i + 1$  are calculated from  $\Delta \theta$  and  $\Delta \ln c$ .

All the coefficients of the model equations in Eqs. (3)–(5) can be estimated by linear regression [3] using the database of historical track records (HurDat), which is maintained by the National Oceanic and Atmospheric Administration (NOAA). The coefficients must be independently derived for each rectangular non-overlapping cell of extension  $5^\circ \times 5^\circ$ , subdividing the Atlantic Ocean region [3]. Moreover, the coefficients are different for east-heading and west-heading hurricanes. For the cells with insufficient historical data, the coefficients of a nearby cell can be used during hurricane simulation. The quantities  $\epsilon_c, \epsilon_\theta$  and  $\epsilon_I$  are linear regression residuals in Eqs. (3)–(5) respectively. Discussion on  $\epsilon_c, \epsilon_\theta$  and  $\epsilon_I$  is provided in the following section.

#### 3.2. Decay model

Once a hurricane lands on the continent, the hurricane can no longer accumulate energy since the source power (sea) has been cut off. The friction between the hurricane system and the ground (land) reduces the hurricane strength. Consequently, the decay of hurricane intensity after landing needs to be modeled; this model, in its simplest form, is [3]

$$\Delta p(t) = \Delta p_0 \cdot \exp(-at_h) \quad (6)$$

The quantity  $\Delta p(t)$  is the hurricane central pressure deficit at time  $t_h$  (in hours) after landing. The quantity  $\Delta p_0$  is the hurricane central pressure deficit at initial landing time ( $t = 0$ ). The parameter  $a$  is an exponential decay rate over time  $t_h$ .

As explained by Vickery and Twisdale [46],  $a$  is a site-specific coefficient which can be related to central pressure deficit  $\Delta p$  as:

$$a = a_0 + a_1 \Delta p + \epsilon_a \quad (7)$$

The term  $\epsilon_a$  is a linear regression residual, which can be modeled as a normal random variable with zero mean. The model for the simulation of hurricane decay intensity, presented in [46], is used in this study. Even though the decay model in Eqs. (6) and (7) has been updated in a more recent study [47], the model in Eqs. (6) and (7) has been widely used by researchers to simulate hurricane decay; this model is believed to be acceptable for the purposes of this investigation and allows other researchers to repeat the simulations, if desired. The  $a_0, a_1$  and the standard deviation  $\sigma_{\epsilon_a}$  of  $\epsilon_a$  are reported in Table 1.

**Table 1**

Exponential decay rate for different sites – reproduced from [46].

Region	$a_0$	$a_1$	$\sigma_{\epsilon_a}$
Florida Peninsula	0.006	0.00046	0.0025
Gulf of Mexico Coast	0.035	0.00050	0.0355
Atlantic Coast	0.038	0.00029	0.0093

### 3.3. Georgiou's gradient wind field model

When a hurricane approaches the continent, it is necessary to estimate the hurricane wind field in order to compute the basic wind speed for structural design purposes. The hurricane wind field can usually be evaluated by aircraft reconnaissance. An aircraft typically records wind speeds at an elevation of 3000 m above the sea surface, which is higher than the gradient wind speed (usually between 500 m and 2000 m [17]). Mature hurricane gradient wind fields can be approximately modeled as a large vortex with a translation movement. Therefore, the gradient wind speed,  $V_g$ , can be decomposed into a rotational component,  $V_R$ , and a translation component,  $V_T$  (Fig. 3).

The rotational component  $V_R$  is assumed to be radially symmetrical about the hurricane eye in this study. Its magnitude depends on the distance  $r$  from the hurricane eye (center). The translation speed  $V_T$  can be found from Eq. (3) and from the track simulations. The resultant gradient wind speed can be determined by vector summation between rotational wind speed and translation speed, as described in the Georgiou's model [1]:

$$V_g = \frac{1}{2}(c \sin \alpha - fr) + \sqrt{\frac{1}{4}(c \sin \alpha - fr)^2 + \frac{100B\Delta p}{\rho} \left(\frac{R_{\max}}{r}\right)^B \exp\left[-\left(\frac{R_{\max}}{r}\right)^B\right]} \quad (8)$$

In Eq. (8)  $c$  is the magnitude of the translation speed,  $\alpha$  is the relative angle between hurricane heading and radial position. The quantity  $R_{\max}$  is the radial distance from the hurricane eye corresponding to maximum winds; it is found from [6]:

$$\ln R_{\max} = 2.63 - 0.000508(\Delta p)^2 + 0.0394\psi + \epsilon_R \quad (9)$$

in which  $\epsilon_R$  is a normal random variable  $N(0, 0.40)$  for all latitudes.

The Holland parameter  $B$  in Eq. (8) is modeled as:

$$B = 1.38 + 0.00184\Delta p - 0.00309R_{\max} \quad (10)$$

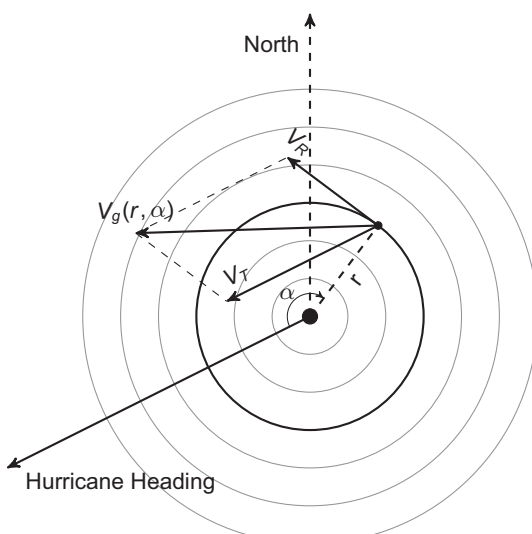


Fig. 3. Hurricane gradient wind field and resultant wind speed.

In the previous equations the units of the quantities are:  $R_{\max}$  and  $r$  in kilometers,  $\Delta p$  in millibar, air density  $\rho$  in  $\text{kg/m}^3$ ;  $f(\text{s}^{-1})$  is the Coriolis parameter. An example of simulated wind speed field, corresponding to the landfall of Hurricane Andrew in Florida in 1992 with the central pressure of 922 millibar ( $\Delta p = 20$  millibar) and heading  $-90^\circ$ , is illustrated in Fig. 4 within a 300 km radius from the hurricane eye center. Because the hurricane is heading west, the maximum speed is observed on the north side of the hurricane eye.

Since hurricanes always rotate counter-clockwise in the northern hemisphere, the maximum wind speed appears at a location where the directions of rotational speed and translation speed are the same. In Fig. 4, the maximum gradient wind speed, obtained from the previous equations, is 65.24 m/s, which is very close to the maximum gradient speed of 64.82 m/s [48], actually recorded at hurricane landing.

### 3.4. Hurricane genesis model: Poisson vs. Negative Binomial

From the analysis of the hurricane historical records and their annual frequencies from 1915 to 2014 in Fig. 5, it is known that the annual frequency is a random process. Currently, two variables and distributions are used to model annual hurricane frequency: Poisson and Negative Binomial. Traditionally, the arrival rate of rare hazards has been described by a Poisson process [2,43,44], which is still employed by several researchers in wind engineering [17,29]. However, Vickery's model in [3] employed the Negative Binomial distribution to model the annual hurricane frequency.

Fig. 6 compares two curves, describing the probability density function (PDF) of the annual hurricane frequency. The PDF curves are derived from the empirical histogram of the data in Fig. 5 by separately fitting the Poisson and the Negative Binomial models. From the inspection of the figure, the Negative Binomial distribution fits the histogram of annual hurricane frequency better than the Poisson distribution. The Poisson distribution usually provides a very "rigid" model curve since it only depends on one parameter; it also assumes that the mean and standard deviation are equal. However, from the historical data the mean of annual hurricane frequency in the North Atlantic region is 13.0, and the standard deviation is 5.84, which is much smaller than the mean value. As a result, there are many discrepancies between the sample histogram and the PDF using the Poisson model. In contrast, the Negative Binomial distribution is more flexible and depends on two parameters. For verification purposes, the one-sample Kolmogorov-Smirnov test [49] is performed on the two fitted distributions. The  $p$ -value is 0.0065 with the Poisson distribution; therefore, the null hypotheses that the Poisson model fits the distribution of the annual hurricane frequency is rejected at the

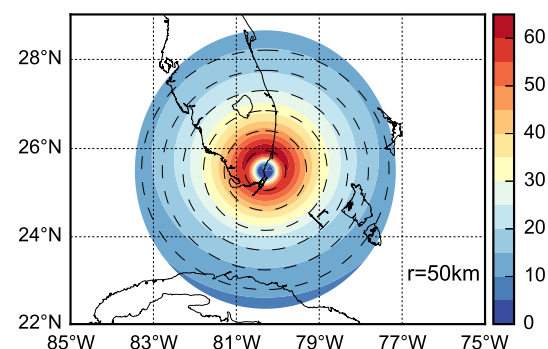
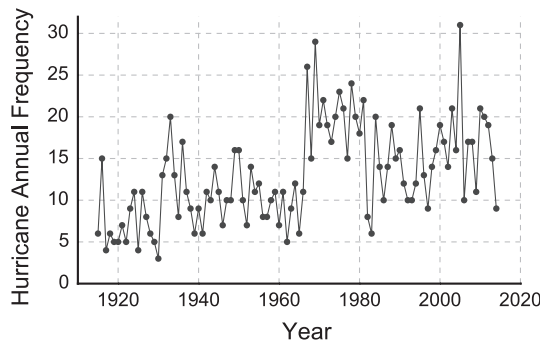
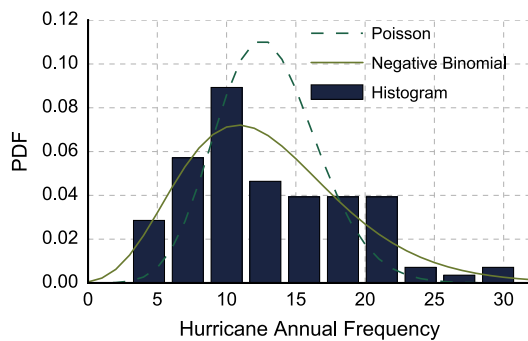


Fig. 4. Simulated gradient wind speed (m/s) field of Hurricane Andrew around its eye when landing close to Miami, FL on August 24, 1992, at 5AM EDT (the radial increment between adjacent concentric circles is 50 km).



**Fig. 5.** Annual hurricane frequency from 1915 to 2014 (HurDat).



**Fig. 6.** PDF of annual hurricane frequency (1915–2014).

$\alpha = 0.05$  confidence level. The  $p$ -value is 0.4516 with the Negative Binomial distribution; therefore the test fails to reject the null hypothesis. Consequently, the Negative Binomial process  $\text{NB}(t : r_{\text{NB}}, p)$  is better suited to model annual hurricane frequency; in this model the parameter  $p$  is the success probability,  $r_{\text{NB}}$  is the number of successes reached before the end of binomial test and  $t$  is the time in years. This variable is later used in the summation term of the cost equation in Eq. (2) instead of the variable  $N(t)$ . It must be noted that the entire HurDat database, which includes events whose maximum intensity corresponds to a tropical depression and not to a fully-developed hurricane, is employed for the hurricane models used in this paper. The Negative Binomial distribution is usually more appropriate to model hurricane genesis. However, removing events that are not of tropical storm intensity or greater significantly reduces the discrepancies between the Poisson and Negative Binomial distributions.

#### 4. Discussion on linear regression errors in Vickery's model

The coefficients used in Eqs. (3)–(5) are determined by linear regression of the historical data, subdivided in  $5^\circ \times 5^\circ$  cells. In addition, the coefficients for west-heading and east-heading hurricanes are different. In the original model [3], limited information on the regression errors related to Eqs. (3)–(5) is provided. In a more recent study [39], several limitations of the linear regression equation, used in Vickery's original model, are pointed out and an alternative simplified approach, based on spatial interpolation, is proposed to model the errors.

Even though discussion on the random error terms  $\epsilon_c$ ,  $\epsilon_\theta$  and  $\epsilon_I$  in Eqs. (3)–(5) is limited, these error terms are crucial for synthetic hurricane simulation, since the randomness of both hurricane tracking and intensity propagation depends on the error terms. In this section, additional discussion is provided and a practical solution is proposed for the treatment of the error terms in the linear regressions.

**Table 2**  
Coefficients obtained by linear regression of historical data through Eq. (3) for the cell located at  $25\text{--}30^\circ\text{N}$ ,  $70\text{--}75^\circ\text{W}$ .

Coefs.	Estimate	Standard error	t-Statistic	p-Value
$a_1$	0.7218	0.5442	1.3265	0.1853
$a_2$	-0.0038	0.0074	-0.5166	0.6057
$a_3$	0.0030	0.0070	0.4329	0.6653
$a_4$	-0.1245	0.0211	-5.8909	$7.5298 \times 10^{-9}$
$a_5$	$8.0887 \times 10^{-4}$	$3.3961 \times 10^{-4}$	2.3817	0.0176

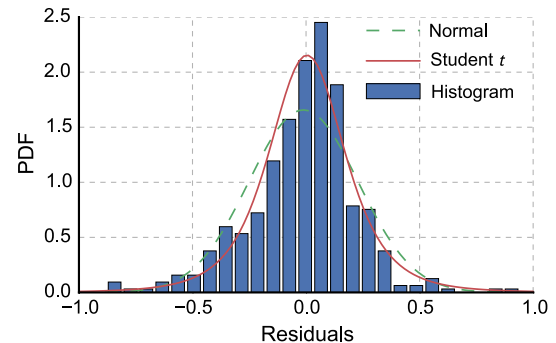


**Fig. 7.** Histogram of residuals and PDF curve, fitted by normal and Student's  $t$ -distributions.

Using the historical data for the cell located at  $(25\text{--}30^\circ\text{N}, 70\text{--}75^\circ\text{W})$  as an example, the linear regression results of Eq. (3) for west-heading hurricanes are examined. A total of 1780 historical hurricanes are used as the sample population for the regression.

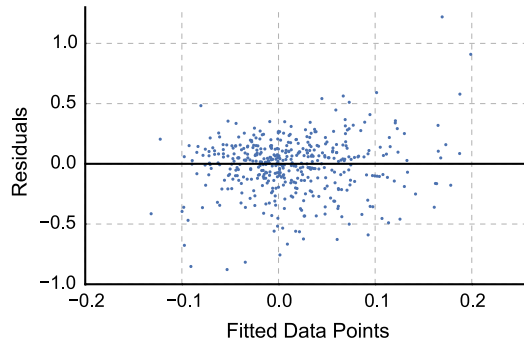
**Table 2** summarizes the estimation of the coefficients in Eq. (3) for this cell. For the coefficients  $a_j (j = 1, 2, \dots, 5)$ , the Student's  $t$  test is performed on the null hypothesis about  $a_j = 0$ . For the  $a_2$  and  $a_3$ , the  $p$ -value are greater than 0.05, which fails to reject the null hypothesis with 95% confidence and casts the doubt about the necessity of including latitude and longitude in Eq. (3), at least for this cell. A similar conclusion was also found by other researchers [39].

Fig. 7 shows the residuals emerging from the linear regression in Eq. (3). The regression residuals are illustrated in Fig. 8; most points are concentrated near the zero line, but there are several points distant from this line. This remark suggests that Eq. (3) cannot fully explain the local variations in the dependent variable  $\Delta \ln c$ . These "unexplained errors" can cause large residuals.

If the normal distribution is used to fit the residuals, The circle markers in Fig. 9 is the Q-Q plot of residual quantiles vs. standard normal distribution. It is observed that there are large discrepancies between theoretical quantiles and sample quantiles in the two tails of the sample. Therefore, it is concluded that the normal distribution is not suitable to model the regression residuals.

The histogram in Fig. 7 reveals the reason why the normal distribution is not a good candidate for modeling residuals. Most residuals are small and near zero. However, a few unexplained large residuals lead to a very flat normal distribution with long tails, which does not comply with the sharp trend in the histogram. As an alternative, the Student's  $t$ -distribution with a third parameter, degrees of freedom, is proposed as a possible better alternative to model the residuals. The degrees of freedom are found during the fitting process in each cell. With the introduction of a third parameter in the PDF model, the Student's  $t$ -distribution more adequately fits both the long tails and the sharp center region.

The Q-Q plot, using Student's  $t$ -distribution as the theoretical quantiles, is depicted as "empty circular markers" in Fig. 9. The comparison between Figs. 7 and 9 illustrates the advantages of the Student's  $t$ -distribution over the normal distribution. The same examination was repeated for other cells and for the regression



**Fig. 8.** Annual hurricane frequency (1915–2014).

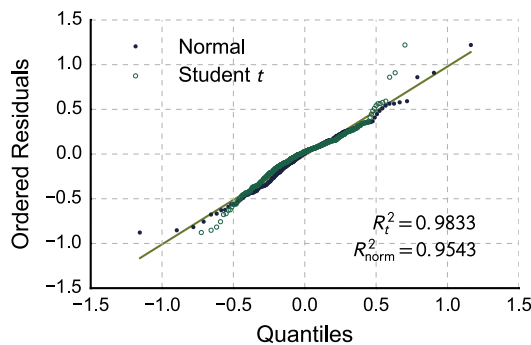


**Fig. 9.** Q–Q plots of regression residuals using standard normal distribution and Student's  $t$ -distribution. The  $R^2$ -squared value is reported on the figure panel for both Student's  $t$ -distribution ( $R_t^2$ ) and normal distribution ( $R_{\text{norm}}^2$ ).

results of Eqs. (4) and (5); similar conclusions and results were noted. More detailed analysis is omitted for the sake of brevity.

To demonstrate the influence in the modeling of error terms, the synthetic simulation of hurricane tracks with the same origin point is illustrated in Fig. 10. The tracks with normally-distributed error terms have greater fluctuations compared to the ones with Student's  $t$ -distributed error terms. The overall agreement with the historical database records of HurDat is better in the second case. As a result, the Student's  $t$ -distribution is employed in the remainder of the study to model the regression error terms.

## 5. Validation of hurricane simulation algorithm

After all the parameters in Eqs. (3)–(5) are determined by linear regression, all historical hurricanes are synthetically simulated from 1915 to 2014 by repeating the simulation 200 times,

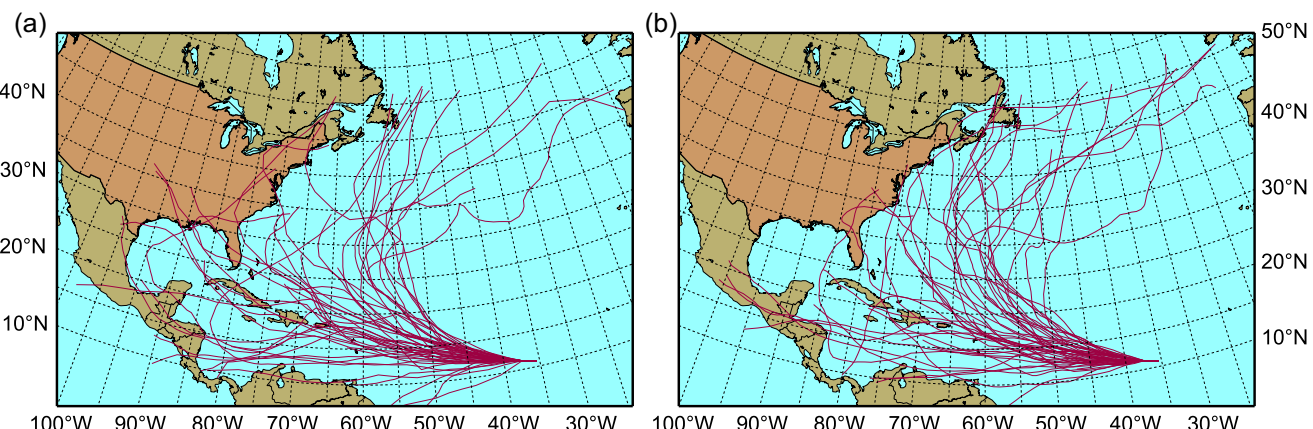
corresponding to a total of 20,000-year simulations. The annual hurricane frequency is considered as a stationary process with constant parameters  $p$  and  $r$ , which are determined as described in the previous section. During hurricane propagation and simulation, the Hadley Centre Global Sea Ice and Sea Surface Temperature dataset (HadISST) [50] is used to provide the SST field data. In order to validate the parameters in Eqs. (3)–(5), the comparisons are given for the statistics of simulated and real hurricanes landed around pre-defined mileposts (MPs) along the US Atlantic coastline. This method was originally proposed by [1] and it is also adopted by [4]. Since the original locations of MPs in [1,4] are not fully available, this study redefines a group of MPs along US coastline starting from the border between US and Mexico near the Gulf of Mexico. All the locations of the MPs are shown in Fig. 11.

Fig. 12 shows 100 randomly selected hurricane tracks, extracted from both the simulation algorithm and the HurDat. Inspection of the figure can hardly distinguish the differences between the two sets.

Detailed statistical comparison (mean values and standard deviations) is presented in Fig. 13 at various MP locations. When a simulated hurricane enters into the 250 km region of the coastal MPs, translation speeds, headings and pressures are recorded. Slight discrepancies between simulation results and HurDat data are observed. The Kolmogorov–Smirnov test [49] is performed at each MP to compare the simulated hurricane speed and heading results against the HurDat data set; the  $p$ -values from the test results are illustrated in Fig. 14. It is found that there are only three MPs (28, 35 and 47) where the test fails at the 0.001 significance level for hurricane heading. Differences appear to be reasonable for the purposes of this study, also because both simulated and real hurricanes are a random process and the HurDat hurricane information is not complete in the early period of the recordings.

For the simulation of the hurricane central pressure, i.e., the coefficient of  $c_j$  in Eq. (5), the simulation result are not statistically compatible with the HurDat records. Therefore, Eq. (5) cannot fully explain the hurricane central pressure development. Using the cell located at (30–35°N, 70–75°W) as an example, the normalized histogram of the regression residuals is plotted in Fig. 15. The shape of the histogram is not a regular “bell”, and it is skewed. The skewness is 0.4933. Therefore, a skewed distribution model is used, if needed, and further parameter adjustment is applied.

Fig. 16 illustrates the mean and RMS values of the hurricane central pressure deficit, obtained by simulation, for all MPs. Similar to the simulation of hurricane speed and heading, small differences exist between simulation results and HurDat records. The Student's  $t$ -test is performed on the simulated hurricane pressure, which are recorded on each MP for comparison with the HurDat



**Fig. 10.** Comparison of hurricane tracks for error terms modeled using normal and Student's  $t$ -distribution: (a) Student's  $t$ -distribution and (b) normal distribution.

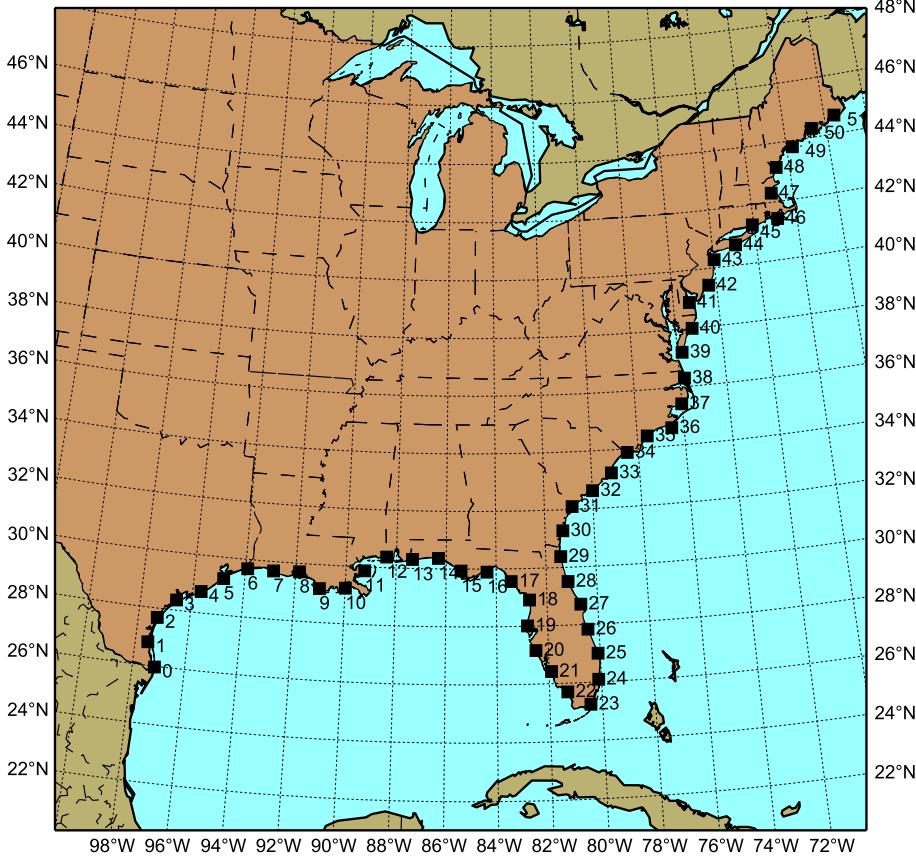


**Fig. 11.** Locations of MPs along the US Atlantic coastline.

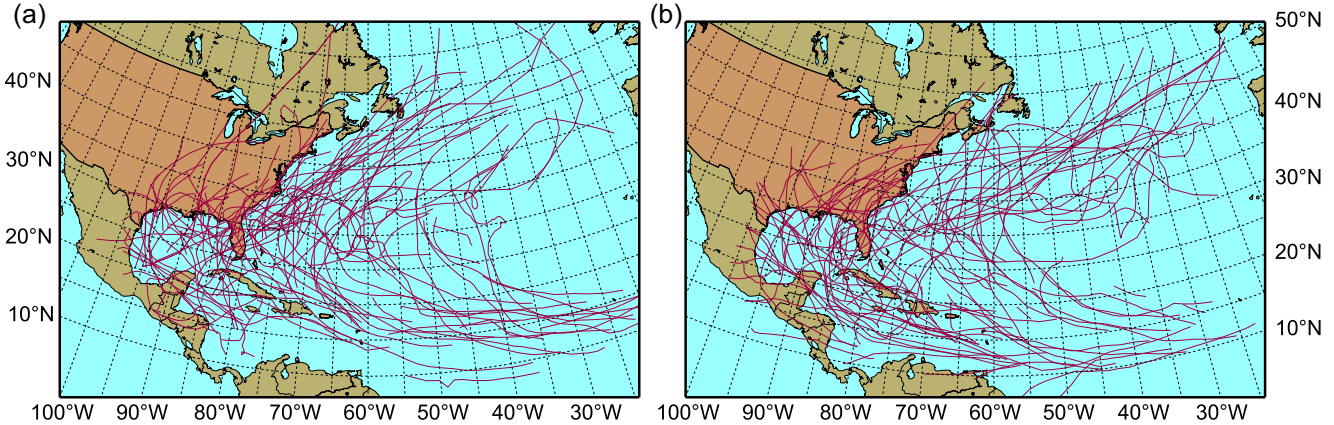


**Fig. 12.** Comparative study of hurricane tracks: (a) historical hurricanes (HurDat) and (b) simulated hurricanes (this model).

records, to further confirm the model accuracy. The statistical test results are listed in Table 3. In all the MPs, the simulation results pass the test at a significance level  $\alpha = 0.05$ , and 45 MPs out of 52 can pass the test at a significance level  $\alpha = 0.20$ . Therefore, it is concluded that the hurricane simulation algorithm is sufficiently accurate and can be applied to the hurricane simulation in warming climate.

## 6. Proposed methodology to estimate structural lifetime costs due to hurricane-induced damage

### 6.1. Hurricane genesis model

After validating the hurricane simulation algorithm in the current climate scenario (i.e., the historical records of HurDat), the

same methodology can be applied to simulate hurricanes in future warming climate scenarios. As previously discussed, a warming climate may have an impact on hurricane genesis frequency, hurricane track, hurricane genesis location and hurricane intensity propagation. A review of the current climatological research in the literature [51,12,52] reveals that hurricane genesis frequency and hurricane intensity propagation are usually examined in detail. Therefore, these two factors are considered in this study.

Since the influence of SST on hurricane genesis location is not directly investigated, the hurricane genesis locations derived from the HurDat records are employed for hurricane simulation in warming climate. All the recorded hurricane genesis locations are plotted in Fig. 17.

For the prediction of hurricane frequency in the remainder of the current century a linear trend model has been used

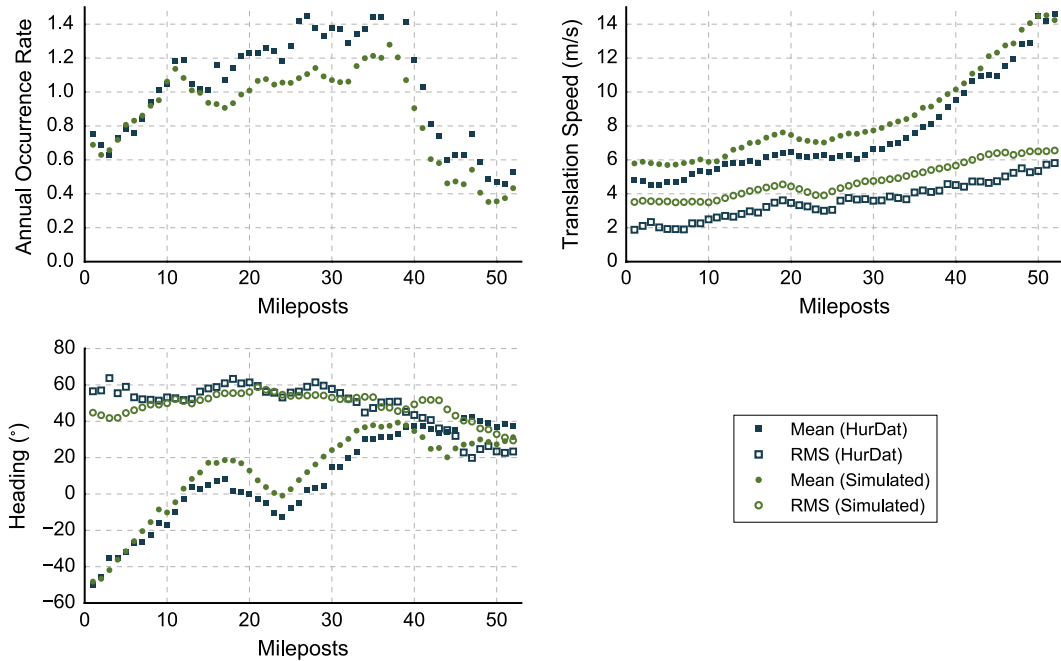


Fig. 13. Validation of simulated hurricane speed, heading and occurrence rate.

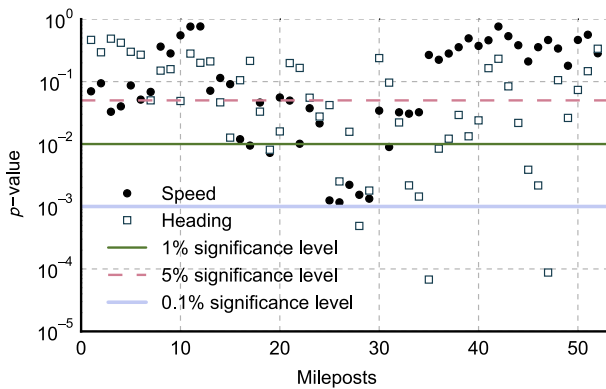


Fig. 14. Kolmogorov-Smirnov statistical test results of simulated hurricane speed and heading (at landfall) against the HurDat data set.

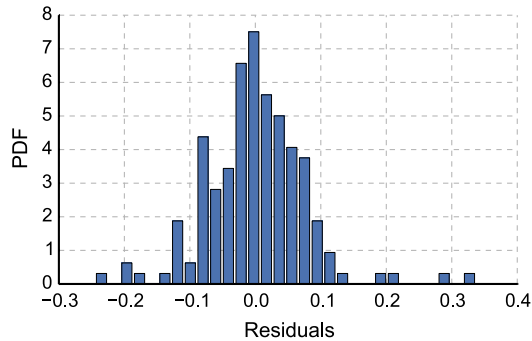
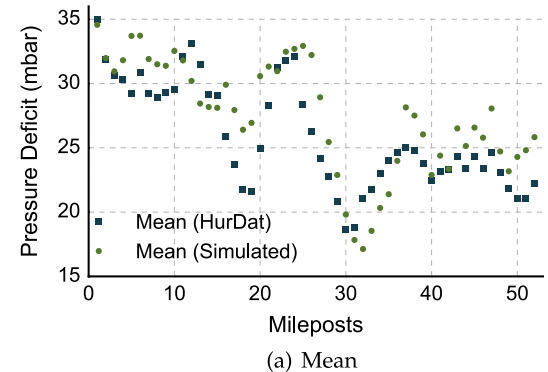
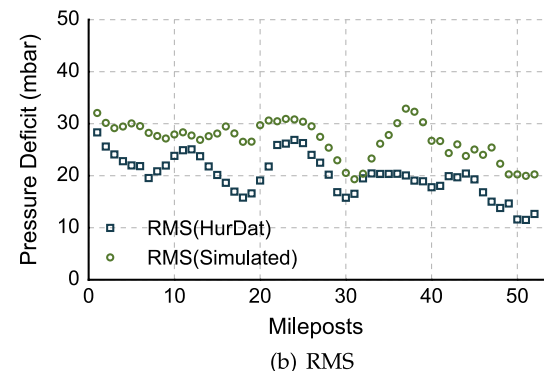


Fig. 15. Histogram of regression residuals using Eq. (5) for the cell located at (30–35°N, 70–75°W).

[17,29,30]. However, several potential issues, rarely discussed by researchers, are possible. One potential problem is related to the fact that much fewer hurricanes have been observed before 1959, corresponding to the year in which the first meteorological



(a) Mean



(b) RMS

Fig. 16. Validation of simulated hurricane central pressure deficit.

satellite was launched. A plausible lack of observations may be responsible for a steeper positive inclination of the regression line in Fig. 18 compared to its real trend. This effect may be perceived from the inspection of Fig. 18. In addition, the time interval used to evaluate the trend on the same figure is relatively short; additional evidence seems to be needed to fully confirm the hypothesis on linear increase. Therefore, a positive linear trend with steep

**Table 3**

Student's *t*-test on simulated hurricane pressure deficit for all MPs.

p-Value	MP number
$0.05 < p < 0.10$	19, 26, 32
$0.10 < p < 0.20$	18, 20, 25, 27
$p > 0.20$	All other MPs

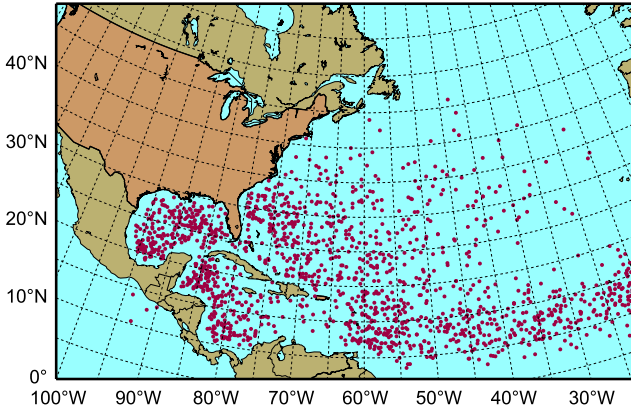


Fig. 17. Hurricane genesis location in the North Atlantic Ocean.

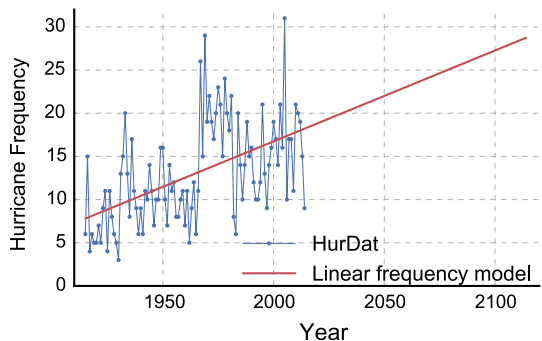


Fig. 18. HurDat hurricane frequency and prediction using linear regression model.

increment may be unsuitable and possibly unrealistic. In atmospheric science, hurricane activities may be related to several climatic indicators [52,12], such as SST, North Atlantic Oscillation, Southern Oscillation and the “El Niño” effect. Although SST is considered the most important factor [51], other factors may have an influence and contribute to the variation of hurricane frequency. This observation would also explain the reduction of hurricane frequency in the time period between 1970 and 1980, despite the global temperature increment in the last century. Due to the inherent difficulties in the prediction of other climatic factors, the “exact” hurricane frequency in a specific year cannot be directly examined. However, from the point view of long-term structural engineering predictions in this study, the use the SST as the only time-dependent climatic factor is acceptable. In [52], a simplified method is proposed to predict the hurricane frequency [51]:

$$\ln \Lambda = \beta_0 + \beta_1 \text{SST}_{\text{Atl}} \quad (11)$$

where the variable  $\text{SST}_{\text{Atl}}$  represents the North Atlantic SST anomalies,  $\Lambda$  is the hurricane frequency and  $\beta_0$  and  $\beta_1$  are constant parameters. The quantity  $\text{SST}_{\text{Atl}}$  is computed for a sea region of latitude between 10°N and 25°N, longitude between 80°W and 20°W, and it is averaged over the period June–November. In this paper Eq. (11) is used to predict the hurricane frequency for the various RCP scenarios from  $\text{SST}_{\text{Atl}}$ .

## 6.2. Proposed framework for hurricane wind forecasting

The second factor, i.e. the influence of an increasing SST, is modeled through Eq. (5). The SST field of the different RCP scenarios uses the simulation results from the Community Climate System Model by NCAR [53], which are publicly accessible. Fig. 19(a) illustrates the average SST field in the north Atlantic Ocean in September 2014. The SST values in the Gulf of Mexico and around the Florida peninsula are higher than the ones in other Ocean regions at the same latitude. Higher SST would lead to more frequent hurricane generation. The figure suggests a higher hurricane occurrence rate around the Gulf of Mexico and the Florida peninsula.

The key step of the structural lifetime cost analysis in Eq. (2) is the quantification of the annual limit state exceedance probability  $P_j$ . The quantity  $P_j$  is computed from the total-probability integral, by cumulating the structural fragility curve with the distribution of annual mean speed maxima of the hurricane winds:

$$P_j = \int_0^\infty F_j(U)f_w(U)dU \quad (12)$$

In the previous equation  $f_w$  is the probability distribution function of the 10-min average wind speed at a reference elevation in hurricanes; the quantity  $F_j(U)$  is the probability that the structural engineering variable  $x_j$ , corresponding to the limit state  $j$ , exceeds the threshold  $T_j$  conditional on the mean wind speed  $U$ , described in Eq. (13) below.

$$F_j(U) = \text{Prob}[x_j > T_j|U] \quad (13)$$

The generic wind speed variable is denoted  $U$  in the previous equations but it is the 10-min mean wind speed at the rooftop of the structure (i.e.,  $\bar{U}(h)$  in Fig. 2).

Traditionally,  $P_j$  has been considered constant over the structural lifetime, i.e. a stationary process. However, in an environment subjected to a changing climate,  $P_j$  may vary over time (e.g., [27,32]) since the  $f_w$  function may change. The hurricane occurrence rate may also vary over time, depending on the RCP scenario according to Eq. (11); therefore, Eq. (12) is modified as:

$$P_j(t) = \int_0^\infty F_j(U)f_w(t, U)dU \quad (14)$$

The flow chart in Fig. 21 summarizes the main steps of the procedure, employed for hurricane generation and to examine structural lifetime intervention costs in warming climate due to damage induced by strong hurricanes. Simulation results and the method to estimate  $f_w(t, U)$  will be discussed in the next section.

Moreover, as shown in Figs. 13 and 16, the hurricane frequency and intensity are geographically and spatially dependent. The gradient wind speeds calculated from Eq. (8) and synthetically simulated hurricanes, are derived for a total of 2728 internal control points (as suggested by Vickery et al. [3]); the points are uniformly distributed with 27.8 km spacing (0.25° on the Earth great circle) and extended to 333.6 km (3° on the Earth great circle) maximum distance from the US Atlantic coastline. These points are shown in Fig. 20. The wind speeds at all other intermediate locations are computed by interpolating the values from the nearest four control points.

## 7. Synthetic hurricane generation: results and discussion

### 7.1. Statistical comparisons at various Mileposts (MPs)

Fig. 22 summarizes the four key factors of the hurricane simulations at each MP under climate change scenarios CP2.6, RCP4.5 and RCP8.5. Results (mean values) are compared to hurricane simulations without the climate change effect. In the RCP2.6 scenario

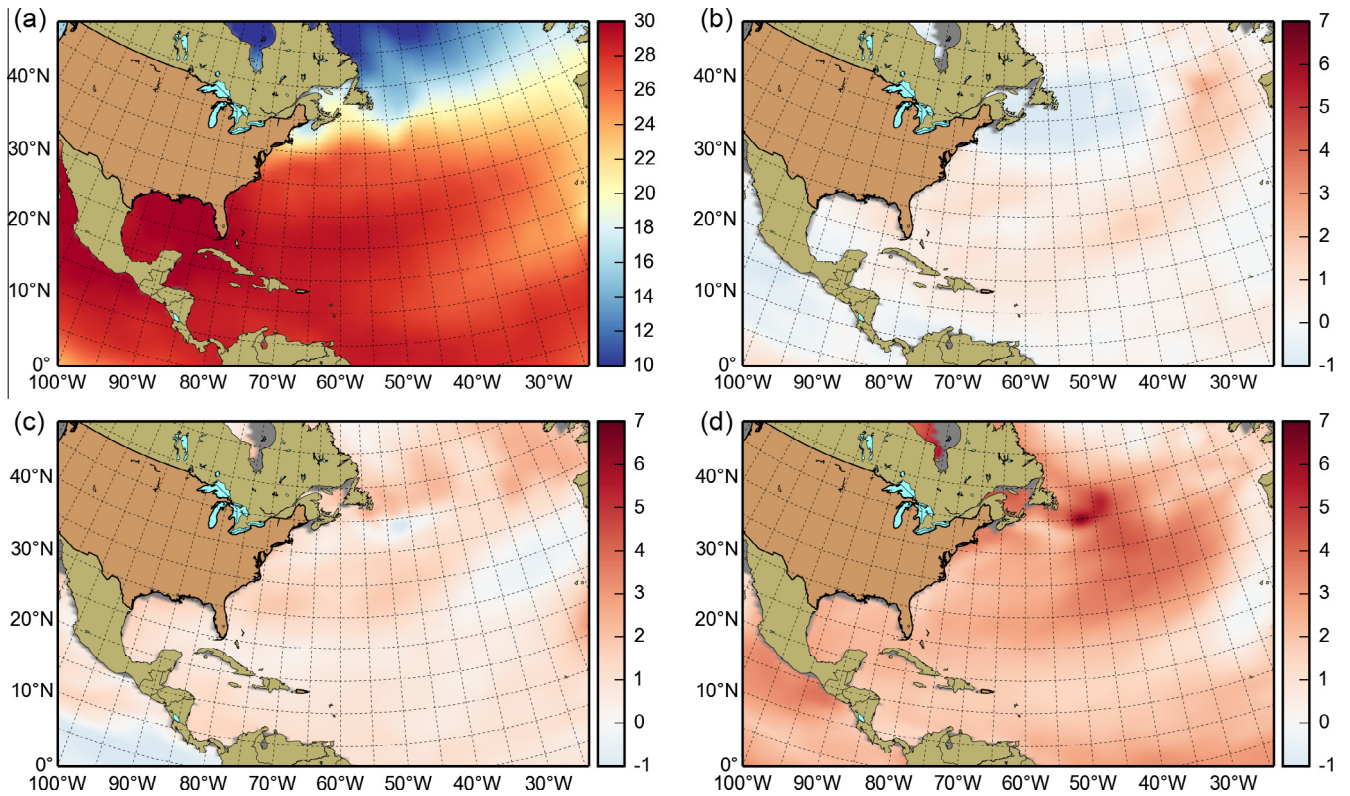


**Fig. 19.** SST observation in September 2014 (a), and projected SST changes in September 2100 under climate change scenarios RCP2.6 (b), RCP4.5 (c), RCP8.5 (d) – reproduced from the Community Climate System Model by NCAR [53].

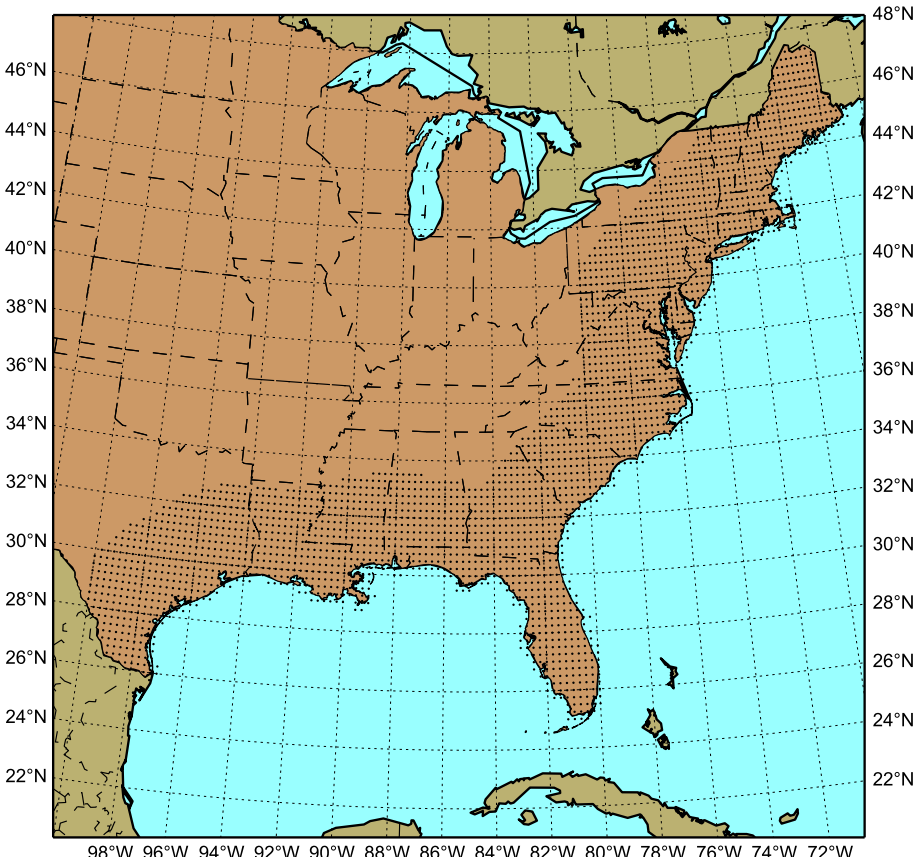


**Fig. 20.** Location of control points for gradient wind speed calculation (stations indicated by “dot” markers).

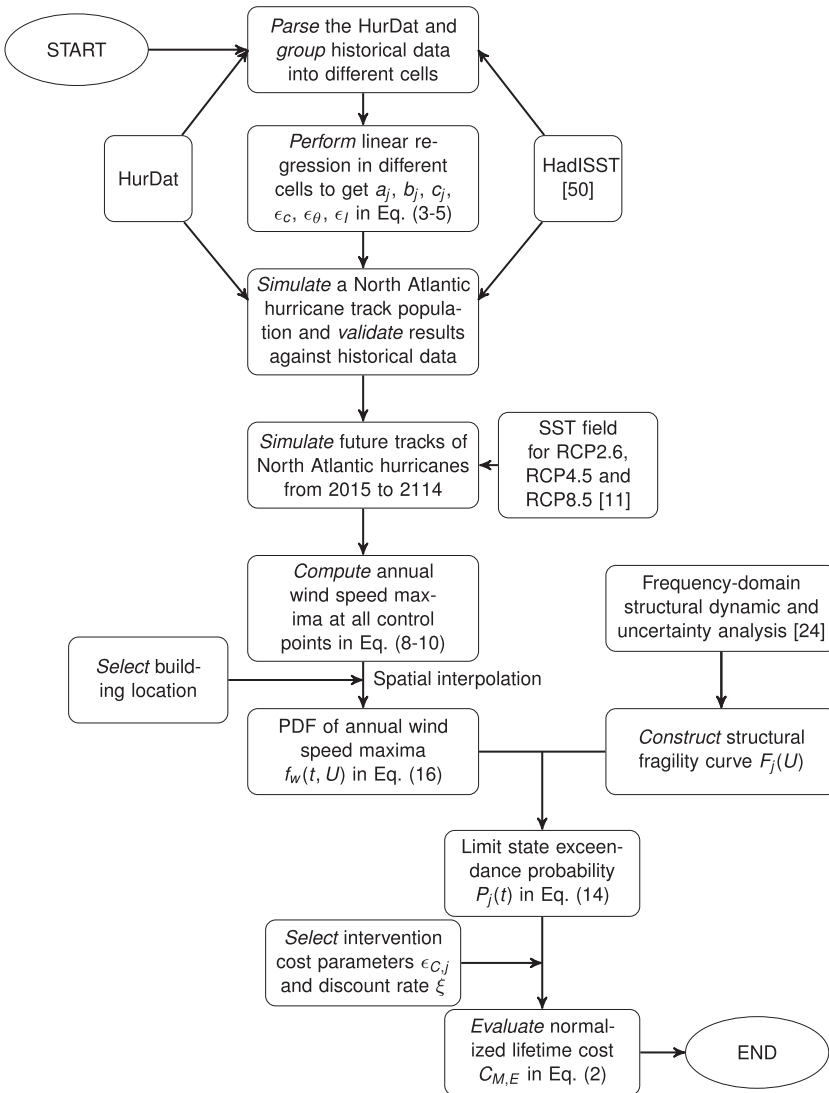


**Fig. 21.** Flowchart of the procedure for examining structural lifetime intervention costs due to hurricane-induced damage in warming climate.

the overall hurricane frequencies are slightly lower than the simulation without climate change because the SST decreases in the last part of the 21st century. However, in the RCP8.5 scenario, hurricane frequency is significantly larger than the other three cases at all MPs (increment between 40% and 60%).

The frequency distribution does not change significantly along the coastline. A small reduction in hurricane frequency is observed for some MPs, especially those in the central part of the Gulf of Mexico and the Atlantic coast around Florida, for RCP2.6 and RCP4.5. The predictions are based on the formula in Eq. (11), which tends to estimate a lower annual frequency in the early years of the 21st century in comparison with the annual average historical frequency obtained from the HurDat. This reduction is influenced by the trade-off between frequency and intensity of global tropical cyclones in a warming climate; a plausible explanation is provided in the literature [54]. More studies would be needed to improve the prediction model for hurricane frequency by taking into account other climatic variables, which have not been considered in this study but may possibly be examined in future studies.

An increment of hurricane pressure deficit is observed with the increase of SST. For example, the RCP8.5 scenario leads to a much higher pressure deficit over all MPs. Since the SST increment is not homogeneous over the whole ocean, the pressure deficit variations are not uniform along the coast. For the MPs from 1 to 6 (western

coast in the Gulf of Mexico) and from 20 to 25 (east side of Florida peninsula) the increment in hurricane pressure deficit is greater (about 15% relative difference with RCP8.5) than the one for other MPs. In the case of RCP2.6 and RCP4.5 scenarios, the relative changes in hurricane pressure deficits appear to be smaller in comparison with the reference case without climate change.

For the hurricane track simulation, results related to the translation speed and heading are marginally influenced by the SST variations. Nevertheless, it is observed that the SST may possibly have an effect on hurricane trajectory; this aspect is beyond the scope of this study and will possibly be considered in future research.

## 7.2. Hurricane gradient wind speed results and comparisons

As discussed in Section 6, hurricane gradient wind speed can be calculated by Eq. (8). The simulated wind speeds are recorded at the control points for each synthetically-generated hurricane. From the sample of the wind speeds the annual maximum of the wind speed can be estimated (year by year). For other locations, not coincident with a control point, the annual maximum wind speed are approximately found by interpolation.

For example, the 200-century sample of the gradient wind speed annual maxima in Miami, Florida (25.78°N, 80.21°W) is plotted as a normalized histogram in Fig. 23.

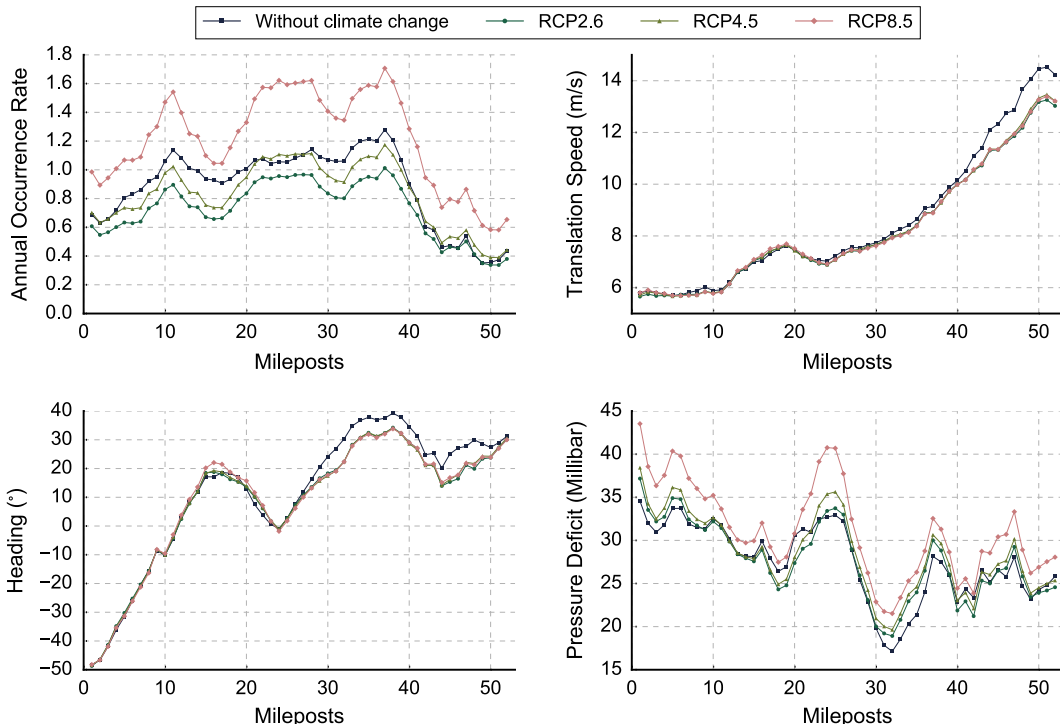


**Fig. 22.** Synthetic hurricane generation: comparison of occurrence rate, speed, heading and pressure deficit using SST from the historical database (without climate change) and SST derived from the NCAR models with RCP2.6, RCP4.5 and RCP8.5.

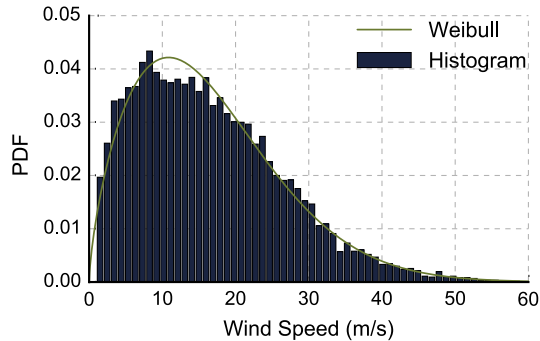


**Fig. 23.** Simulated annual gradient wind speed maxima distribution (m/s) at Miami, Florida (USA).

In Fig. 23, the Weibull distribution is used to fit the empirical histogram of the wind speed, as defined in Eq. (15):

$$f_w(U; \eta, k) = \frac{k}{\eta} \left(\frac{U}{\eta}\right)^{k-1} \exp\left[-\left(\frac{U}{\eta}\right)^k\right] \quad (15)$$

In the previous equation  $\eta$  is the scale parameter,  $k$  is the shape parameter and  $U$  denotes gradient wind speed.

Inspection of the figure reveals that the Weibull fitting agrees with the sample histogram. The Chi-squared statistical test [55] is used to examine the hurricane wind speed data set at Miami and the hypothesis of Weibull probability distribution. The test results indicate that Weibull probability distribution function for hurricane wind speed passes the test at a significance level 0.05 since  $p = 0.0948$ . In [2], the Weibull model is also recommended for approximating the distribution of the hurricane annual maximum wind speed. In a similar way, the simulated annual maximum wind speed distribution can be determined in the case of future climates. The empirical histograms for each RCP are not shown for the sake of brevity. The fitted Weibull distributions, depending on the various RCP scenarios, are compared to the

simulated curve without the effect of climate change in Fig. 24 for the same location (Miami).

The warming climate scenario RCP2.6 has a hurricane wind speed distribution very similar to the current scenario. Most importantly, in the case of the RCP8.5 scenario, which replicates the worst case predicted by NCAR models, the distribution curve has a clearly distinct shape: the median point shifts to larger speeds and the upper tail becomes thicker and more skewed.

As described in Section 6 a non-stationary process is proposed to model the variations of annual wind speed maxima in the warming climate. From Eq. (15) a modified Weibull distribution with time-dependent parameters  $\eta(t)$  and  $k(t)$  is proposed in Eq. (16) below:

$$f_w(t, U; \eta(t), k(t)) = \frac{k(t)}{\eta(t)} \left(\frac{U}{\eta(t)}\right)^{k(t)-1} \exp\left[-\left(\frac{U}{\eta(t)}\right)^{k(t)}\right] \quad (16)$$

The 200-century repeated simulations of annual wind speed maxima are regrouped according to the simulation year, by progressively varying the SST in accordance with the NCAR projections for the corresponding year. In each year, the Weibull distribution is fitted to the simulated sample of annual wind speeds and used to estimate the parameters  $k(t)$  and  $\eta(t)$ . The results of  $k(t)$  and  $\eta(t)$  for each future RCP scenario and the current climate are illustrated in Fig. 25. The simulated data points resemble the behavior of a “scatter plot” because of the inherent stochastic nature of annual maximum wind speed.

In order to investigate the overall trend over time, simulation results are fitted over time by linear regression. For the RCP8.5 scenario, the two parameters  $k(t)$  and  $\eta(t)$  are clearly time dependent and they both increase with time. For the RCP4.5 scenario, the increasing trend of  $k(t)$  and  $\eta(t)$  is still present, although the trend lines are considerably flatter than the RCP8.5 trend. In the case of the RCP2.6 scenario, the trend line of the shape parameter  $k(t)$  is almost horizontal and similar to the reference line obtained for non-warming climate. A very small dependence of  $\eta(t)$  on time is

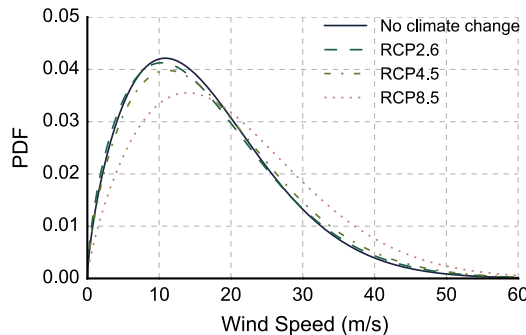


**Fig. 24.** Gradient wind speed: Weibull distribution comparison (Miami, Florida) between the three RCP scenarios and the simulation without the effect of climate change.

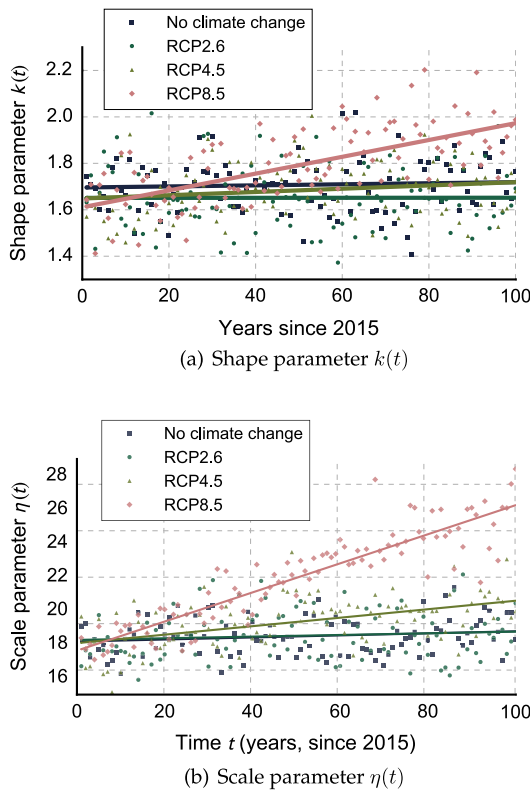


**Fig. 25.** Time-dependent Weibull distribution parameters  $k(t)$  and  $\eta(t)$  for warming climate for Miami, Florida.

observed in the RCP2.6 curve. It is concluded that the stationary process hypothesis can still be used to evaluate structural vulnerability in the case of both RCP2.6 scenario and non-warming climate. However, the non-stationary processes should be employed with the RCP4.5 and RCP8.5 scenarios. In the next section an example will demonstrate the complete methodology for the evaluation of structural vulnerability and lifetime intervention cost under the simulated effects of climate change.

## 8. Projecting the effects of hurricane wind speed in future warming climate on the lifetime intervention costs of a benchmark tall building

### 8.1. Description of the benchmark building and derivation of limit state exceedance probabilities

In this section, the benchmark tall building of the Commonwealth Advisory Aeronautical Council (CAARC) [56] is selected as

the first prototype application of the proposed methodology. This building has been used in wind engineering as a standard building model for comparison among various wind tunnel experimental data and analysis techniques. Fig. 26 illustrates a schematic view of the CAARC building with an indication of the main dimensions (depth  $D$ , width  $B$ , height  $h$ ).

Fig. 2 reports the structural fragility curves, estimated for the two limit states of peak lateral displacement at the rooftop ( $z = h$ ) and RMS acceleration at the rooftop. In the case of the CAARC building the reference mean wind speed, used by the fragility analysis and reported on the horizontal axis of Fig. 2, is  $\bar{U}(h)$  at  $h = 183$  m. The estimation of these curves for the CAARC building is described in a recent study [24] and it is not reported for the sake of brevity.

Before the cost analysis, the wind speed obtained from simulated hurricanes must be converted from gradient wind speed to wind speed near the ground surface, i.e.,  $\bar{U}(h)$  in this example. The gradient-to-surface conversion factor is taken from Batts et al. [57]. In particular, the CAARC building is assumed to be located in open terrain corresponding to exposure category C in ASCE 7-10 [58]. Supplementary validation of the synthetic annual maximum wind speed is carried out by comparing the present results with the results from the hurricane model by Batts et al. [57]. The simulated hurricane wind speeds at four selected locations along the US eastern coastline are compared against the literature values [57] for various recurrence intervals ( $\bar{N}$ ) in Table 4. In Table 4, the hurricane wind speeds for the three climate change scenarios are also listed.

The results in Table 4 suggest that the simulated wind speeds at the four selected MPs in the scenario without climate change are compatible with the predictions by Batts et al. [57]. The same four locations will be employed in the second part of this sub-section and in the next sub-section for the structural vulnerability analyses. The results are sufficiently accurate for the four MPs but may need to be supplemented by additional studies to confirm the validity of the synthetic hurricane simulation for other locations.

For the uncertainty analysis, the limit state exceedance probability over time (Eq. (14)) is computed by using the gradient wind speed distribution parameters in Fig. 25 and the fragility curves in Fig. 2. Limit state exceedance probabilities are shown in Fig. 27.

In Fig. 27 the  $P_1(t)$  curve corresponds to the peak lateral drift or deformation limit state and the  $P_2(t)$  curve is the RMS acceleration

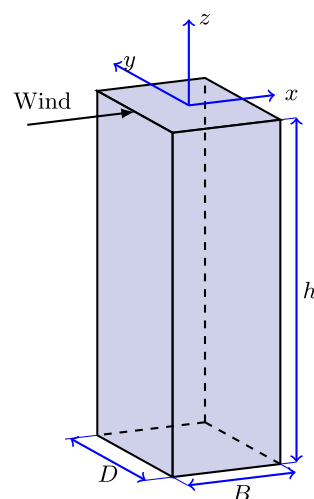


**Fig. 26.** Schematic view of the CAARC building (depth  $D$ , width  $B$ , height  $h$ ).

**Table 4**

Estimated hurricane 10-min wind speeds (m/s) at 10 m above ground in open terrain at selected locations along US coastline as a function of mean recurrence interval  $\bar{N}$ .

Location	Miami, FL					New Orleans, LA				
	i	ii	iii	iv	v	i	ii	iii	iv	v
$\bar{N} = 25$ yr	<b>31.4</b>	<b>28.6</b>	29.4	30.8	35.5	<b>27.6</b>	<b>28.2</b>	26.2	26.7	29.3
$\bar{N} = 50$ yr	<b>33.3</b>	<b>29.4</b>	30.8	34.6	39.0	<b>30.5</b>	<b>31.5</b>	29.6	30.3	32.8
$\bar{N} = 100$ yr	<b>36.2</b>	<b>36.8</b>	35.4	38.0	42.2	<b>33.3</b>	<b>34.6</b>	33.2	33.4	36.2
Norfolk, VA					New York, NY					
$\bar{N} = 25$ yr	<b>21.9</b>	<b>23.8</b>	24.1	24.7	27.2	<b>21.0</b>	<b>21.0</b>	20.8	21.9	25.8
$\bar{N} = 50$ yr	<b>25.7</b>	<b>27.7</b>	28.1	28.6	30.9	<b>28.6</b>	<b>25.1</b>	25.3	26.5	30.1
$\bar{N} = 100$ yr	<b>30.5</b>	<b>30.9</b>	31.5	32.2	33.9	<b>32.4</b>	<b>28.8</b>	29.1	30.6	34.6

Case **i**: Reference value from the hurricane model by Batts et al. [57].

Case **ii**: Simulated value from the present model without climate change.

Case **iii**: Simulated value from the present model for RCP2.6 scenario.

Case **iv**: Simulated value from the present model for RCP4.5 scenario.

Case **v**: Simulated value from the present model for RCP8.5 scenario.

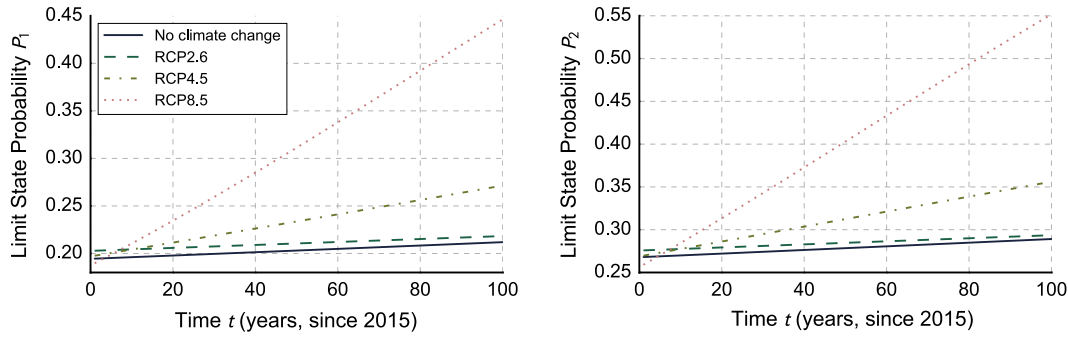


Fig. 27. Structural limit states of the CAARC building, located in Miami (Florida): exceedance probability over lifetime caused by strong hurricane winds.

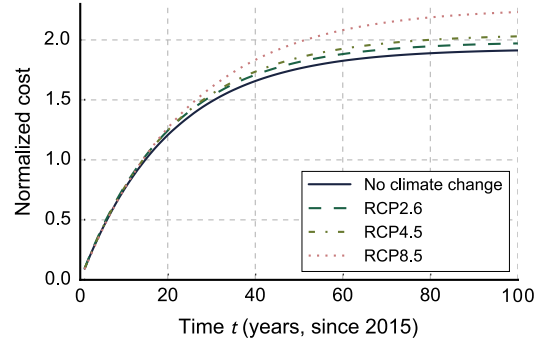


Fig. 28. Influence of warming climate on the normalized intervention cost of the CAARC building, located in Miami (Florida).

limit state. The threshold limits respectively are  $h/400$  ( $T_j = T_1$  in Eq. (13)) and 5 milli-g ( $T_j = T_2$  in Eq. (13)) [24]. Both exceedance probabilities are strongly time dependent in the case of RCP4.5 and RCP8.5 scenarios. For RCP2.6, the increasing trend is not obvious as with the two other, more severe, warming climate scenarios. In the case of the scenario without climate change the SST field, extracted from the HadISST database from 1915 to 2015, exhibits an increasing trend over time. Therefore, although the hurricane frequency is constant, this trend in the SST field of HadISST causes the  $P_1(t)$  and  $P_2(t)$  to increase very slowly over time.

## 8.2. Intervention cost analysis in a warming climate

After substituting  $P_1(t)$  and  $P_2(t)$  obtained from Fig. 27 into Eq. (16), the normalized intervention cost results can be derived from

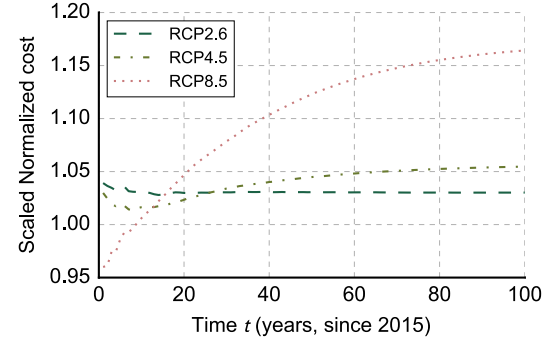
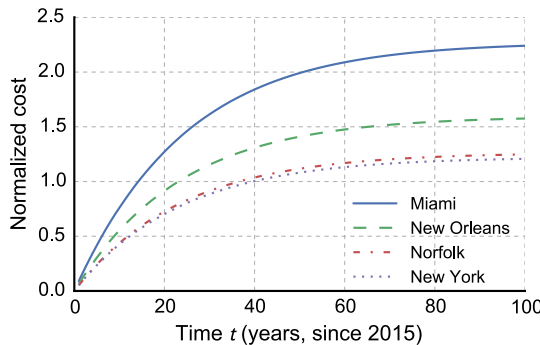


Fig. 29. Intervention cost analysis for the CAARC building, located in Miami (Florida), re-scaled to the reference cost without the effect of climate change (continuous line in Fig. 28).

Eq. (2) with  $\epsilon_{C,1}$  and  $\epsilon_{C,2}$  assumed to be 0.2 [24]. Numerical results are illustrated in Fig. 28.

Fig. 29 presents the cost result re-scaled to the cost without the effect of climate change (the continuous line in Fig. 28) to examine the cost variation depending on the various RCP scenarios. In most warming climate scenarios the relative increment of the cost in comparison with the reference scenario is of the order of 10%; the variation becomes +30% after 100 years with RCP8.5.

Finally, the above-described procedure was used to evaluate the effects of a warming climate for the same building at other locations along the US coastline. Fig. 30 shows the results of the cost analysis, limited to the RCP8.5 scenario, when the location of the CAARC building is moved to other major cities along the southern or eastern coast of the United States. From the curves in Fig. 30 it is



**Fig. 30.** Influence of climate change (RCP8.5 scenario) on the intervention cost results for the CAARC building, located in various major coastal cities of the US (Miami, New Orleans, Norfolk, New York).

concluded that Miami is the most vulnerable site to the effects of hurricanes in warming climate. New Orleans has lower hurricane damage because most hurricanes usually travel a short distance across the Gulf of Mexico before reaching New Orleans. Damage due to storm surge effects is not considered in this model. When the anticipated damage is exclusively related to wind effects (no surge), much lower hurricane damage (about 50% compared to other locations) is predicted in cities such as Norfolk and New York in the mid-Atlantic and northeastern regions of the US coast.

### 8.3. Discussion of the results

Even though the cost estimation is based on a set of nominal unit costs  $\epsilon_{Cj}$  [24], it is believed that the simulation results are valuable in relative terms. They suggest that an increment in the cost is possible over time, between 10% and +30% depending on the RCP scenario. This relative variation is perhaps small in comparison with other sources of uncertainty, which could possibly more severely influence the structural performance over time, such as building deterioration and regular maintenance. It is also recalled that cost estimation is based on the concept of cost evaluated in present dollar value and that the discount factor  $\xi$  was conventionally set to 5% in the simulations. The  $\xi$  factor reduces the severity of a strong wind event happening in the distant future. In any case, this type of analysis is relevant since it demonstrates the typical “temporal scale” of the effects associated with a warming climate. The relatively small cost variations in Fig. 29 are in fact plausible since this temporal length scale may be longer than the lifetime of the structure.

## 9. Conclusions

This paper describes the derivation of a framework for estimation of lifetime intervention costs on tall structures due to hurricane-induced damage in warming climate by using a state-of-art statistical hurricane track model [3]. The structural cost analysis [28,24] is applied to the performance of the CAARC benchmark tall building, located in Miami and other US coastal cities. The synthetic hurricane simulation makes use of the sea surface temperature (SST) field in the Atlantic Ocean, resulting from three RCP scenarios and climate simulation SST results reproduced from the Community Earth System Model [53].

In the first part of this study an investigation on the regression random errors in Vickery's hurricane-track model was described. It is concluded that the Student's *t*-distribution instead of the normal distribution [17,39] is preferable to model the random errors.

The second part of the study presented the implementation of a numerical methodology for the synthetic hurricane simulation, which depends on the temporal variability of SST. This variability

indirectly accounts for the effect of warming climate in accord with various RCP scenarios. The procedure replicates the spatial fluctuations of SST over time in various regions of the Atlantic Ocean in line with the most recent accurate climatological studies [53], instead of considering a constant and uniform SST variation [17]. In the third part of this study the SST influence on hurricane frequency in warming climate is indirectly evaluated. The annual hurricane frequency was derived from year-by-year averages of SST. These averages can be adapted to comply with the different RCP scenarios and account for more realistic fluctuations in the model [53], which are more accurate than the simple linear regression of annual hurricane frequency over time [27,17,29,30]. The hurricane simulation results suggest that both hurricane frequency and hurricane intensity will increase in the future, and the increments largely depend on the RCP scenarios.

After hurricane track simulation, the hurricane gradient wind speeds was evaluated by using Georgiou's model at several control points located in the US Atlantic coastal region. Finally, after combining the gradient wind speed distribution extracted for a specific site with existing fragility analysis information on the benchmark building, the study examined the structural lifetime intervention costs due to hurricane damage for a number of warming climate scenarios [53]. Similar to a standard cost analysis in the absence of climate change effects, the intervention costs in warming climate asymptotically tend to an upper limit, as time increases, due to the effect of the discount factor [28,24].

Future investigations should account for hurricane wind speed and direction since wind loads and structural response are strongly influenced by both wind speed and wind direction. Furthermore, the simulation of hurricanes in warming climate should possibly include the SST effect on hurricane trajectory path and genesis location as well as the influence of other environmental factors, such as wind shear, tropopause temperature and humidity. These are other important supplementary issues related to the SST effect on hurricane intensity. Finally, the track model used for synthetic hurricane generation might need further investigation. Either the adjustment of the parameters in the existing model or an upgraded model could possibly improve the overall accuracy in the simulations.

## Acknowledgments

This material is based upon work supported in part by the National Science Foundation (NSF) of the United States under CAREER Award CMMI-0844977 in 2009–2014. The support of MathWorks Inc. through a micro-grant awarded by Northeastern University (NEU) and Professor Miriam Leeser (Department of Electrical and Computer Engineering, NEU) in 2015 is also gratefully acknowledged. Any opinions, findings and conclusions or recommendations are those of the authors and do not necessarily reflect the views of either the NSF or any other sponsor.

## References

- [1] Georgiou PN, Design wind speeds in tropical cyclone-prone regions, Ph.D. dissertation. University of Western Ontario, London, Ontario, Canada; 1986.
- [2] Simiu E, Scanlan RH. Wind effects on structures: fundamentals and applications to design. 2nd ed. New Jersey, USA: John Wiley & Sons; 1986.
- [3] Vickery P, Skerlj P, Twisdale L. Simulation of hurricane risk in the U.S. using empirical track model. J Struct Eng 2000;126(10):1222–37.
- [4] Vickery PJ, Skerlj P, Steckley A, Twisdale L. Hurricane wind field model for use in hurricane simulations. J Struct Eng 2000;126(10):1203–21.
- [5] Emanuel K, Ravela S, Vivant E, Risi C. A statistical deterministic approach to hurricane risk assessment. Bull Am Meteorol Soc 2006;87(3):299–314.
- [6] Lee KH, Rosowsky DV. Synthetic hurricane wind speed records: development of a database for hazard analyses and risk studies. Nat Hazards Rev 2007;8 (2):23–34.
- [7] Powell M, Soukup G, Cocke S, Gulati S, Morisseau-Leroy N, Hamid S, et al. State of Florida hurricane loss projection model: atmospheric science component. J Wind Eng Ind Aerodynam 2005;93(8):651–74.

- [8] Vickery PJ, Wadhena D, Twisdale Jr LA, Lavelle FM. US hurricane wind speed risk and uncertainty. *J Struct Eng (ASCE)* 2009;135(3):301–20.
- [9] Vickery PJ, Wadhena D, Galsworthy J, Peterka JA, Irwin PA, Griffis LA. Ultimate wind load design gust wind speeds in the united states for use in ASCE-7. *J Struct Eng (ASCE)* 2009;136(5):613–25.
- [10] Houghton J, Jenkins G, Ephraums J. Report prepared for intergovernmental panel on climate change by working group I. Cambridge, Great Britain: Cambridge University Press; 1990.
- [11] Stocker TF, Qin D, Plattner GK, Tignor M, Allen SK, Boschung J, et al. Climate change 2013: the physical science basis. Tech. rep., 2013. 1535 pp.
- [12] Villarini G, Vecchi GA. Twenty-first-century projections of North Atlantic tropical storms from CMIP5 models. *Nat Clim Change* 2012;2(8):604–7.
- [13] Webster PJ, Holland GJ, Curry JA, Chang HR. Changes in tropical cyclone number, duration, and intensity in a warming environment. *Science* 2005;309(5742):1844–6.
- [14] Stewart MG, Wang X, Nguyen MN. Climate change impact and risks of concrete infrastructure deterioration. *Eng Struct* 2011;33(4):1326–37.
- [15] Santillán D, Salete E, Toledo M. A methodology for the assessment of the effect of climate change on the thermal-strain-stress behaviour of structures. *Eng Struct* 2015;92(0):123–41.
- [16] Kölöi A, Pakkala TA, Lahdensivu J, Kivistö M. Durability demands related to carbonation induced corrosion for Finnish concrete buildings in changing climate. *Eng Struct* 2014;62–63(0):42–52.
- [17] Mudd L, Wang Y, Letchford C, Rosowsky D. Assessing climate change impact on the U.S. east coast hurricane hazard: temperature, frequency, and track. *Nat Hazards Rev* 2014;15(3):04014001.
- [18] van de Lindt J, Dao T. Performance-based wind engineering for wood-frame buildings. *J Struct Eng* 2009;135(2):169–77.
- [19] Li Y, Ellingwood BR. Hurricane damage to residential construction in the US: importance of uncertainty modeling in risk assessment. *Eng Struct* 2006;28(7):1009–18.
- [20] Barbato M, Petrini F, Unnikrishnan VU, Ciampoli M. Performance-based hurricane engineering (PBHE) framework. *Struct Saf* 2013;45(0):24–35.
- [21] Spence SM, Gioffrè M. Large scale reliability-based design optimization of wind excited tall buildings. *Probab Eng Mech* 2012;28:206–15.
- [22] Spence SM, Kareem A. Performance-based design and optimization of uncertain wind-excited dynamic building systems. *Eng Struct* 2014;78:133–144. [Performance Based Engineering: Current Advances and Applications].
- [23] Bashor R, Kareem A. Probabilistic performance evaluation of buildings: an occupant comfort perspective. In: Proceedings of the 12th international conference on wind engineering.
- [24] Cui W, Caracoglia L. Simulation and analysis of intervention costs due to wind-induced damage on tall buildings. *Eng Struct* 2015;87(0):183–97.
- [25] Smith MA. A Monte Carlo based method for the dynamic performance analysis of tall buildings under turbulent wind loading; 2009.
- [26] Ciampoli M, Petrini F. Performance-based aeolian risk assessment and reduction for tall buildings. *Probab Eng Mech* 2012;28:75–84.
- [27] Seo DW, Caracoglia L. Exploring the impact of “climate change” on lifetime replacement costs for long-span bridges prone to torsional flutter. *J Wind Eng Ind Aerodyn* 2015;140(0):1–9.
- [28] Seo DW, Caracoglia L. Estimating life-cycle monetary losses due to wind hazards: fragility analysis of long-span bridges. *Eng Struct* 2013;56:1593–606.
- [29] Mudd L, Wang Y, Letchford C, Rosowsky D. Hurricane wind hazard assessment for a rapidly warming climate scenario. *J Wind Eng Ind Aerodyn* 2014;133(0):242–9.
- [30] Lee JY, Ellingwood BR. Intergenerational risk-informed decision framework for civil infrastructure. In: Deodatis G, Ellingwood BR, Frangopol DM, editors. Safety, reliability, risk and life-cycle performance of structures and infrastructures. CRC Press/Balkema; 2014. p. 3369–74.
- [31] Liu F. Projections of future us design wind speeds due to climate change for estimating hurricane losses, Ph.D. dissertation. Clemson University, Clemson, South Carolina; 2014.
- [32] Lee JY, Ellingwood BR. Impacts of climate change on long-term risk to building structures exposed to hurricanes. In: EMI 2014 – engineering mechanics institute conference. American Society of Civil Engineers; 2014.
- [33] Van Vuuren DP, Edmonds J, Kainuma M, Riahi K, Thomson A, Hibbard K, Hurtt GC, Kram T, Krey V, Lamarque JF. The representative concentration pathways: an overview. *Climatic Change* 2011;109:5–31.
- [34] Emanuel KA. The dependence of hurricane intensity on climate. *Nature* 1987;326(6112):483–5.
- [35] Goldenberg SB, Landsea CW, Mestas-Nuñez AM, Gray WM. The recent increase in Atlantic hurricane activity: causes and implications. *Science* 2001;293(5529):474–9.
- [36] Vickery PJ, Lavelle FM. The effects of warm Atlantic Ocean sea surface temperatures on the asce 7–10 design wind speeds. *Bridges* 2014;10. 9780784412626-002.
- [37] Vickery PJ, Masters FJ, Powell MD, Wadhena D. Hurricane hazard modeling: the past, present, and future. *J Wind Eng Ind Aerodyn* 2009;97(7):392–405.
- [38] DeMaria M, Knaff JA, Kaplan J. On the decay of tropical cyclone winds crossing narrow landmasses. *J Appl Meteorol Climatol* 2006;45(3):491–9.
- [39] Li S, Hong H. Observations on a hurricane wind hazard model used to map extreme hurricane wind speed. *J Struct Eng* 2014.
- [40] Inokuma A. Basic study of performance-based design in civil engineering. *J Prof Issues Eng Educ Pract* 2002;128(1):30–5.
- [41] Ellingwood B, Rosowsky D, Li Y, Kim J. Fragility assessment of light-frame wood construction subjected to wind and earthquake hazards. *J Struct Eng* 2004;130(12):1921–30.
- [42] Smith MA, Caracoglia L. A Monte Carlo based method for the dynamic “fragility analysis” of tall buildings under turbulent wind loading. *Eng Struct* 2011;33(2):410–20.
- [43] Seo DW, Caracoglia L. Statistical buffeting response of flexible bridges influenced by errors in aeroelastic loading estimation. *J Wind Eng Ind Aerodyn* 2012;104:129–40.
- [44] Wen YK, Kang YJ. Minimum building lifecycle cost design criteria. I: methodology. *J Struct Eng (ASCE)* 2001;127(3):330–7.
- [45] Darling R. Estimating probabilities of hurricane wind speeds using a large-scale empirical model. *J Clim* 1991;4(10):1035–46.
- [46] Vickery PJ, Twisdale LA. Wind-field and filling models for hurricane wind-speed predictions. *J Struct Eng* 1995;121(11):1700–9.
- [47] Vickery PJ. Simple empirical models for estimating the increase in the central pressure of tropical cyclones after landfall along the coastline of the united states. *J Appl Meteorol* 2005;44(12):1807–26.
- [48] Hladny WG, Quenemoen LE, Armenia-Cope RR, Hurt KJ, Malilay J, Noji EK, et al. Use of a modified cluster sampling method to perform rapid needs assessment after hurricane Andrew. *Ann Emerg Med* 1994;23(4):719–25.
- [49] Massey Jr FJ. The Kolmogorov-Smirnov test for goodness of fit. *J Am Stat Assoc* 1951;46(253):68–78.
- [50] Rayner NA, Parker DE, Horton EB, Folland CK, Alexander LV, Rowell DP, et al. Global analyses of sea surface temperature, sea ice, and night marine air temperature since the late nineteenth century. *J Geophys Res: Atmos* 2003;108(D14):4407.
- [51] Villarini G, Vecchi GA, Knutson TR, Zhao M, Smith JA. North Atlantic tropical storm frequency response to anthropogenic forcing: projections and sources of uncertainty. *J Clim* 2011;24(13):3224–38.
- [52] Villarini G, Vecchi GA, Smith JA. Modeling the dependence of tropical storm counts in the North Atlantic basin on climate indices. *Mon Weather Rev* 2010;138(7):2681–705.
- [53] National Center of Atmospheric Research (NCAR) Community Earth System Model. <<http://www2.cesm.ucar.edu/>> [accessed: 2015-06-02].
- [54] Kang NY, Elsner JB. Trade-off between intensity and frequency of global tropical cyclones. *Nat Clim Change* 2015;5(7):661–4.
- [55] Yates F. Contingency tables involving small numbers and the  $\chi^2$  test. *Suppl. J. R. Stat. Soc.* 1934;217–35.
- [56] Melbourne WH. Comparison of measurements on the CAARC standard tall building model in simulated model wind flows. *J Wind Eng Ind Aerodyn* 1980;6(1):73–88.
- [57] Batts ME, Simiu E, Russell LR. Hurricane wind speeds in the united states. *J Struct Div* 1980;106(10):2001–16.
- [58] ASCE. Minimum design loads for building and other structures (ASCE 7-10); 2010.